Icarus 241 (2014) 130–147

Contents lists available at ScienceDirect

Icarus

journal homepage: www.elsevier.com/locate/icarus

Timescales of fluvial activity and intermittency in Milna Crater, Mars

Peter B. Buhler [a,*], Caleb I. Fassett [b], James W. Head III [c], Michael P. Lamb [a]

[a] California Institute of Technology, MC 170-25, Pasadena, CA 91126, USA
[b] Department of Astronomy, Mount Holyoke College, 50 College St, South Hadley, MA 01075, USA
[c] Brown University, Department of Geological Sciences, Providence, RI 02912, USA

ARTICLE INFO

Article history:
Received 23 January 2014
Revised 11 June 2014
Accepted 25 June 2014
Available online 3 July 2014

Keywords:
Mars, surface
Geological processes
Mars, climate

ABSTRACT

Milna Crater, Mars (23.4S, 12.3W) exhibits signs of fluvial modification early in Mars history, including a large multi-lobed fan deposit cut by several sinuous valleys. We describe the past hydrologic conditions in Milna and the surrounding area, including a potential lake with a volume of 50 km^3. We also introduce new methods (i) to calculate the timescale of sediment deposition by considering fluvial sediment input into the entire crater while accounting for non-fluvial input, and (ii) to place improved constraints on the channel dimensions through which sediment was delivered to Milna by comparing to the dimensions of inner channels found in valleys in the region surrounding Milna. By calculating the flux of fluid and sediment into the crater, we find that the crater cavity was flooded for at least months and that the time of active fluvial sediment transport without hiatus is on the order of decades to centuries, with a preferred timescale of centuries. We also calculate the total amount of water required to transport the volume of sediment we measure in Milna and conclude that impacts alone are likely insufficient to deliver enough water to Milna to allow the sedimentary fill we see.

Combining the timescales of fluvial activity in the adjacent Paraná Valles with estimates for global Noachian erosion rates, we calculate an intermittency factor for fluvial activity of ~0.01–0.1% during 10^5–10^6 yr near the Noachian–Hesperian boundary in the Paraná Valles region. These values are comparable to arid climates on Earth where the majority of fluvial sedimentary transport takes place during floods with multi-year to decadal recurrence intervals. Our calculations of intermittency help to quantitatively reconcile the divergent estimates of the short and long timescales of fluvial activity on Mars reported in the literature.

1. Introduction

Ancient lake deposits and valley networks on Mars provide strong evidence that its surface was once modified by liquid water (e.g. discussions in Craddock and Howard, 2002; Gaidos and Marion, 2003; Moore et al., 2003; Burr et al., 2009; Carr, 2012), but the extent of that modification is still a subject of intense deliberation. One of the most important, and most debated, variables pertaining to ancient hydrological activity on Mars is the timescale over which it operated.

Over the past several decades the question of timescales of fluvial modification of the martian surface has been approached from the local, regional, and global perspectives. Although there is evidence that both valley networks and outflow channels (e.g., Baker and Milton, 1974; Pieri, 1980; Carr and Clow, 1981) provided water for the formation of lakes (e.g. De Hon, 1992; Cabrol and Grin, 1999), the lakes sourced by valley networks appear to have formed under conditions that were closer to equilibrium climate conditions than lakes formed in a different epoch by catastrophic outflow (e.g. Fassett and Head, 2008b; Carr, 2012).

One approach employed to calculate the time over which fluvial activity redistributed sediment on the martian surface involves measuring the volume of a sedimentary fan or delta and dividing that volume by an estimated flux of waterborne sediment into a basin (e.g. Moore et al., 2003; Jerolmack et al., 2004; Bhattacharya et al., 2005; Kleinhans, 2005; Metz et al., 2009; Kleinhans et al., 2010; Schon et al., 2012; DiBiase et al., 2013). A number of investigations into fluvial timescales related to valley networks and their associated lake and fan deposits have yielded a wide range of estimates for the timescales over which fluvial modification has taken place, from local processes operating over less than years (e.g. alluvial fans: Kleinhans et al., 2010) to global and regional modification lasting hundreds of millions of years (e.g. modeling of crater erosion, Craddock and Howard, 2002); see Table 1.

On Earth there are also orders of magnitude difference in timescale for formation of fluvial landforms, which can be explained both by hiatus in fluvial activity and by the fact that Earth does

* Corresponding author.
E-mail address: bpeter@caltech.edu (P.B. Buhler).

http://dx.doi.org/10.1016/j.icarus.2014.06.028
0019-1035/

Nomenclature

A	drainage area, m^2	Φ	sediment flux, $m^3\ s^{-1}$
A_L	paleolake area, m^2	φ	porosity, dimensionless
b	shape-fitting parameter for fresh crater cavity, dimensionless	Q	fluid flux, $m^3\ s^{-1}$
C_1	coefficient describing grain shape, dimensionless	R	hydraulic radius of channel, m
C_2	coefficient describing grain shape, dimensionless	R_s	submerged specific gravity of sediment, dimensionless
d	crater depth, km	r	element roughness scale for a fixed bed (e.g. bedrock), m
d_{rm}	crater depth after being filled with eroded rim material, km	S	slope, dimensionless
D	crater diameter, km	T	timescale to build sedimentary fill, s
D_{50}	50% clasts have smaller diameters than this value, m	t_p	timing of a precipitation event, s
D_{84}	84% clasts have smaller diameters than this value, m	T_e	erosion time, s
D_S	sediment diameter, m	T_{min}	timescale to flood crater, s
E	erosion rate, m/s	τ_*	shields stress, dimensionless
ε	evaporation rate, m/s	U	mean fluid velocity in channel, $m\ s^{-1}$
f_c	Darcy–Weisbach friction factor for channel, dimensionless	u^*	shear velocity, $m\ s^{-1}$
f_p	bankfull storm event period, s	V_C	current crater cavity volume, m^3
g	martian gravitational acceleration, $m\ s^{-2}$	V_{inlet}	volume of inlet channel, m^3
h	depth of fluid in channel, m	V_0	fresh crater cavity volume, m^3
H	rim height, km	V_S	volume of sedimentary fill, m^3
k	suspended:bedload flux ratio, dimensionless	ν	kinematic viscosity, $m^2\ s^{-1}$
L	fraction of precipitation runoff lost to evaporation, dimensionless	W	width of channel, m
P	precipitation depth, m	w_S	terminal settling velocity, $m\ s^{-1}$
ρ_f	fluid density, assumed to be 1000, $kg\ m^{-3}$	x	radial distance extending from the center of the crater, km
ρ_S	sediment density, assumed to be 2800 (cf. Daly et al., 1966), $kg\ m^{-3}$	X	X-ratio comparing precipitation and evaporation rates (Matsubara et al., 2011)
		z	vertical distance relative to lowest point in fresh crater, m

not experience constant storm conditions—rather, fluvial modification of the landscape happens periodically (e.g. Wolman and Miller, 1960). Knowledge of the terrestrial water cycle has led several authors (e.g. Moore et al., 2003; Jerolmack et al., 2004; Bhattacharya et al., 2005; Fassett and Head, 2005; Kleinhans, 2005; Barnhart et al., 2009; Metz et al., 2009; Schon et al., 2012) to invoke periodic recurrence of fluvial processes to explain the formation of fluvial landforms on Mars. However, so far, constraints on the frequency of periodic reworking of sediment on Mars are weak (e.g. Carr, 2012).

This study focuses on the problem of constraining the timescale over which fluvial processes operated to input sediment into Milna Crater (23.4S, 12.3W; in the Margaritifer Sinus Quadrangle; Fig. 1). This approach differs from others in that sediment input into the entire crater, rather than just into a fan, is considered. We also introduce improved methods for estimating the dimensions of

Table 1
Summary of timescale estimates performed for Mars. The timescale under which fluvial processes operated, as interpreted by the author (named in the 'study' column) is listed under 'timescale.' A brief description of the features observed and methods used to determine this timescale is also given. The work done by Craddock and Howard (2002) models the total timescale under which fluvial processes were active on Mars, while the locally formed events refer to timescales under which fluvial processes acted to form specific features, such as fans and deltas.

Timescale (yr)	Method	Study
Locally formed events		
<1–1	Alluvial fan formation, no hiatus	Kleinhans et al. (2010)
10^1	Stepped delta formation, single event	Kraal et al. (2008)
10^1–10^2	Paleolakes/deltas, ~20 yr with no hiatus to a factor of 20 longer, assuming hiatus like in humid climates on Earth	Jerolmack et al. (2004)
10^1–10^3	Fluid discharge rates constrained by Jezero Crater morphology, similar hiatus assumptions to Jerolmack et al. (2004)	Fassett and Head (2005)
10^2	Ebeswalde delta formation via fluid bearing a high sediment concentration, continuous deposition	Mangold et al. (2012)
$\geqslant 10^2$	Delta formation at Aoelis Dorsa (no hiatus)	DiBiase et al. (2013)
10^2–10^4	Alluvial fans with varying hiatus (10^1–10^4 yr) based on comparisons to terrestrial turbidites	Metz et al. (2009)
10^3–10^4	Comparison of martian deltas with terrestrial delta timescales	Mangold and Ansan (2006)
10^3–10^6	Eberswalde delta formation with discussion of possible hiatus scenarios	Moore et al. (2003)
10^5	Eberswalde deposit, with major flows occuring every ~10^2 yrs and assuming mm/yr sediment input	Bhattacharya et al. (2005)
10^5–10^6	Computer simulation of valley development in Paraná Valles (near Milna)	Barnhart et al. (2009)
10^5–10^7	Valley network erosion rates (timescale range from continuous flow to flow 1% of the time)	Hoke et al. (2011)
<~10^6	Valley development in Paraná Valles (near Milna)	Irwin et al. (2007)
<~10^6–10^7	Interactions between craters and river channels at Aoelis Dorsa	Kite et al. (2013)
10^6–10^7	Depositional morphology of the Jezero Crater delta, comparison to terrestrial timescales	Schon et al. (2012)
10^6–10^8	Model of alluvial fan formation, with estimation of sediment availability based on erosion timescales	Armitage et al. (2011)
Other comparisons		
<10^2	Fans in Saheki Crater recording 100s of small flows during the Late Hesperian–Early Amazonian	Morgan et al. (2014)
10^3–10^6	Regional outflow rates of valleys compared to sedimentary structures	Kleinhans (2005)
<10^3–10^7	Terrestrial lake lifetimes, from dammed lakes (<10^3) to lakes in tectonic rift zones and periglacial environments (10^7)	Cohen (2003)
10^8	Erosion and crater removal modeling	Craddock and Howard (2002)

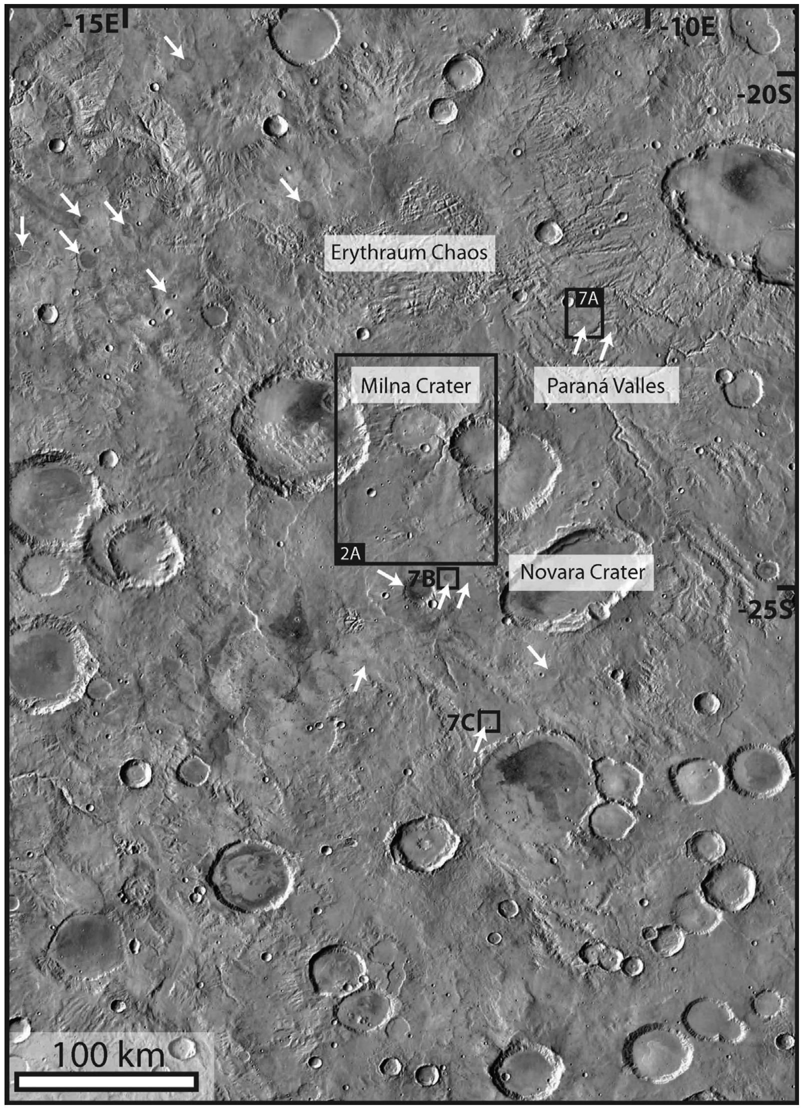

Fig. 1. Milna Crater is a crater with a 27 km diameter, centered at (23.4S, 12.3W). It is located just south of Paraná Vallmalized by the submerged grain weight peres and Erythraeum Chaos, and northwest of Novara Crater. Arrows denote the locations of ghost craters (see Fig. 7). The locations of Figs. 2A and 7A–C are indicated. *THEMIS IR mosaic.*

channels inputting sediment. Finally, the location of Milna Crater near the well-studied Paraná Valles (e.g. Howard et al., 2005; Barnhart et al., 2009) and the presence of a large, well-defined drainage area, allows a contextualization of the timescale of sediment input into Milna and permits a calculation of the percentage of the time over which significant fluvial activity took place.

Milna Crater has been interpreted as an open basin paleolake (see Irwin et al., 2005b; Fassett and Head, 2008b). An open basin paleolake is a depression, such as a crater, that has a valley sloping into it (an *inlet* valley) and a valley leading out of it (an *outlet* valley), often accompanied by other signs of fluvial modification (e.g. Goldspiel and Squyres, 1991; Cabrol and Grin, 1999; Irwin et al., 2007; Fassett and Head, 2005, 2008b; Buhler et al., 2011). Evidence for a paleolake in Milna Crater was first discovered by Irwin et al. (2005b). Unlike most open basin paleolakes (see Carr, 2012), Milna contains a fan deposit with several lobes that are incised by several sinuous valleys, akin to Eberswalde (Malin and Edgett, 2003; Wood, 2006) and Jezero (Fassett et al., 2007) craters. This deposit allows us to qualitatively demonstrate that the sedimentary fan records a multi-stage history and to quantitatively calculate the timescales of fluvial activity in Milna.

In this paper we first make the case that Milna once housed an open basin paleolake and qualitatively describe its history (Section 3). Second, we enumerate the techniques we employ to calculate the timescales of sedimentary fill construction, contrasted with the time to simply flood the crater with fluid (Section 4). Third, after considering the impact of non-fluvial modification of Milna (Section 5), we present numerical estimates of the minimum and maximum timescales of fluvial activity (Section 6), including calculations of hiatus timescales and recurrence intervals (Section 7). Finally, we contextualize our findings within the discussion of the ancient global climate on Mars (Section 8).

2. Methods

Orbital missions to Mars in the past decade have supplied us with detailed information on the topography and morphology of the martian surface. For topographic information, we made use of Mars Orbiter Laser Altimeter (MOLA) 1/128 pixel per degree gridded data (463 m/px) (Smith et al., 2001). Geomorphic information was primarily derived from the Context Camera (CTX) (Malin et al., 2007) image data at resolution ~6 m/px. To augment CTX data, we used Thermal Emission Imaging System (THEMIS) (Christensen et al., 2003) VIS (~18 m/px) and IR (100 m/px) images, and nadir HRSC (Neukum et al., 2004) data (up to 12.5 m/px). High Resolution Imaging Science Experiment (HiRISE)

(McEwen et al., 2007) images (0.25 m/px) were also used in available locations. The data were compiled and co-registered in the ArcMap GIS environment using the USGS ISIS software package.

We used a combination of morphologic data and topographic data to identify inlet and outlet valleys and determine the direction of their local slope. The maximum surface area and volume possible for a paleolake in Milna Crater, with the current geometry of the crater, was obtained by finding the highest elevation closed contour in the crater. The topography within this closed contour was then extracted to enable direct measurement of the surface area at, and volume of the crater below, a surface constructed at the elevation of the inlet and outlet valleys. All values given for elevations refer to the height above the current lowest point Milna, which corresponds to −1040 m relative to the mean global martian surface elevation derived from the MOLA dataset.

In order to determine the amount of post-impact fill in Milna, theoretical fresh crater dimensions were calculated using the equations found in Garvin et al. (2002) (see Section 4.1). The theoretical values obtained from these equations were checked by comparison to two fresh craters that are approximately the same diameter as Milna, centered at (5.0S, 53.0E, 26.2 km diameter) and (5.7S, 35.9E, 25.4 km diameter). The current cavity volume, V_C, was calculated by constructing a reference surface over Milna at the elevation of the surrounding plains and then calculating the volume between the current crater floor and that surface. We created a high resolution digital terrain model (DTM) using the Ames Stereo Pipeline (Moratto et al., 2010) of CTX images P01_001586_1563 and P01_001388_1563 that provides high resolution topography over the fans, but did not cover the entire crater; thus we use MOLA DTMs for calculations of the geometry of the whole crater.

Fans are identified by their convex, rounded scarps (e.g. Williams and Malin, 2008; Metz et al., 2009; Carr, 2012). The drainage basins were determined in ArcMap GIS environment using the 'Basin' tool, after creating a flow direction raster using the 'Flow Direction' tool based on the MOLA gridded dataset and eliminating spurious sink points with the 'Fill' tool. Valley versus inner channel ratios were calculated by measuring both the valley width and the inner channel width at 15 evenly spaced locations from the first point at which the inner channel is resolvable until the inner channel was no longer resolvable, along the midline between the valley walls for the valley and the midline between the channel walls for the channel, using the Measure tool in ArcMap GIS. The mean of each of these measurements were taken, and the channel:valley ratio is given by the mean channel width divided by the mean valley width. Average valley slopes were calculated by measuring the length of the valleys along a line centered between the walls of the valley, and then dividing that length by the difference in elevation—obtained from the MOLA 1/128 pixel per degree gridded dataset—between the two ends of the valley. Slopes in this paper are generally smooth and reported for elevation changes of tens to hundreds of meters over valleys with lengths ~10 km or greater. Since MOLA has a vertical accuracy of ~1 m (Smith et al., 2001), we estimate that errors of the slope estimate are a few 10^{-4} and so measurement error should not significantly impact the slope estimates. Calculations of timescale estimations, channel dimension, crater fill, and intermittency are given in Sections 4–7.

3. Description and interpretation of Milna Crater

3.1. Post-impact modification and evidence for a paleolake

Milna Crater is centered at (23.4S, 12.3W), in the Margaritifer Sinus Quadrangle, just south of Paraná Valles (Fig. 1). There is a valley that slopes into Milna from the southeast, and a valley that slopes out of Milna toward the northwest; we interpret these as an inlet and an outlet valley, respectively, because of the inferred direction of water flow based on the average valley slopes (Fig. 2). Also, in addition to the inlet and outlet valleys, there is another, less incised valley to the west of Milna that slopes into the crater, which we interpret as a secondary inlet valley because it is less deeply cut than the other two valleys (Fig. 2D). The highest closed contour around Milna is 275 m (Fig. 2D); correlatively, the lowest open contour around Milna is 280 m, which is opened by its intersection with the outlet valley to the west.

Milna has been extensively modified since its formation. The crater rim is eroded and incised; in addition to the outlet valley, main inlet valley, and secondary inlet valley, there are smaller valleys modifying the rim (Fig. 2D). Milna Crater also likely contains a large amount of fill based on a comparison of the present topographic profile across Milna and the ideal cavity shape for fresh craters (Fig. 3; see Section 4). Sedimentary fill sources in Milna are discussed in greater detail in Section 5. There are also several lobate features and sinuous valleys in the interior of the crater (Fig. 4). Since the elevations of the outlet valley breach, the top of the sedimentary deposit, and the inlet valley breach correlate well (Fig. 2), and we assume that the current crater topography is similar today to the crater topography when the breaches formed, we conclude that water flowed in and out of the crater simultaneously and thus there was a lake in Milna (cf. Fassett and Head, 2008b).

To the south of Milna there is a broad basin with several shallow incisions leading into it (Fig. 5A). We interpret this basin as a location where surface water ponded (Fig. 2B). A short, well-defined sinuous valley leads to a broad valley that slopes downhill and becomes more tightly confined to the north, eventually leading to the sharp scarp that marks the beginning of the deep valley that leads into the Milna cavity (Figs. 2 and 5A). These valleys suggest that this southern basin, together with Milna, formed a chain of two paleolakes.

3.2. Paleohydrology

Using the maximum closed contour as the maximum water surface level, measurements of the geometry of Milna in its current state, partially filled with sediment, show that it has the capability to hold 50 km^3 of water, with a surface area of 410 km^2 (see Table 2). In its early state, prior to infilling with sediment, it would have been able to hold up to 316 km^3 of water, as calculated from theoretical fresh crater dimensions (see Table 2, Section 4). These volumes are not unusual when considered against estimates of volumes of other martian paleolakes (e.g. Grin and Cabrol, 1997; Malin and Edgett, 2003; Bhattacharya et al., 2005; Ehlmann et al., 2008; Fassett and Head, 2008b; Di Achille et al., 2009; Buhler et al., 2011).

We assume that the fluvial modification of Milna took place contemporaneously with the fluvial activity in nearby Paraná Valles since Milna is located in the catchment of Paraná Valles (see Barnhart et al., 2009; Fig. 1); this fluvial modification terminated at approximately the Noachian–Hesperian Boundary (Fassett and Head, 2008a). Thus Milna provides insight into the fluvial activity leading up the Noachian–Hesperian Boundary.

3.3. Reconstruction of fluvial sedimentary deposition

Milna Crater exhibits a sedimentary deposit with many lobes and several valleys that incise into these lobes (Fig. 4). We map five distinct depositional lobes; this is a minimum because we group some depositional lobes into the same unit and other lobes may be buried or modified beyond recognition by erosion (Fig. 4). Although the lobes are spatially distinct depositional units, care must be taken not to necessarily interpret temporal separation

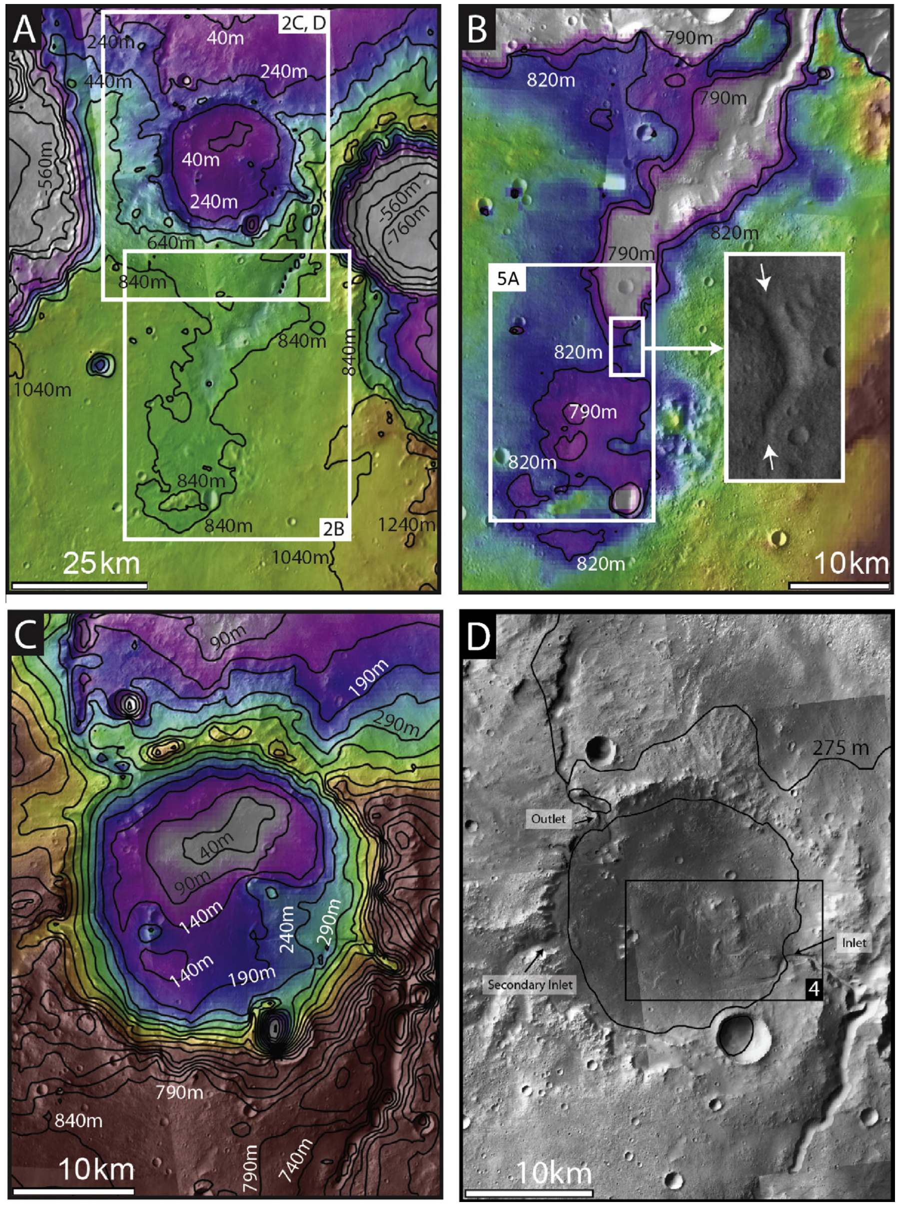

Fig. 2. (A) The contours are given relative to the lowest point in Milna Crater (global elevation of −1040 m). Context given for (B–D). (B) A basin closed by an 820 m contour is connected to a broad valley by a small sinuous valley (inset). The broad valley narrows to become the inlet valley to Milna (top right corner). Context for Fig. 5A is given. (C) 50 m contours at Milna Crater. The contours bulge out on the fans (southeast corner). (D) The highest closed contour around Milna is at 275 m (black contour), it is breached by the outlet valley at an elevation of 280 m. There are two inlet valleys to Milna; one has a well-developed fan (see Fig. 4), and one (secondary) does not have a definitive fan, but the valley becomes unconfined by definite walls at an elevation of 290 m. Note also the knobby rim of the crater and that the outlet valley incises fill material for several kilometers before exiting the crater. *Image is (A) THEMIS IR mosaic, elevation from MOLA, CTX (P01_001586_1563, P14_006465_1582), THEMIS VIS (V19060005, V16614006, V16302005); 200 m contour interval. (B) THEMIS IR mosaic, elevation from MOLA, CTX (P01_001586_1563), THEMIS VIS (V26685008, V15990002, V15079004, V14767002, V16614006, V16302005); inset THEMIS VIS (V14767002). (C) THEMIS IR mosaic, elevation from MOLA, CTX (P01_001586_1563, P14_006465_1582), THEMIS VIS (V19060005, V16614006, V16302005); 50 m contour interval. (D) THEMIS IR mosaic, contour from MOLA, CTX (P01_001586_1563, P14_006465_1582), THEMIS VIS (V19060005, V16614006, V16302005); inset CTX (P01_001586_1563).*

between units or differences in climate during their deposition, because that cannot be determined solely from the presence of multiple lobes (for instance, the Mississippi delta on Earth has formed six lobes during the Holocene under a fairly stable climate and sea-level; see Roberts, 1997). The inlet and outlet valleys of Milna exhibit sinuous morphology and monotonic slope (.011 and .005, respectively); the outlet valley is partly inverted (Fig. 5A; cf. Williams et al., 2009). The co-occurrence of sinuous valleys leading into the crater and multiple depositional lobes indicate that fluvial erosion and deposition significantly modified Milna (cf. Goldspiel and Squyres, 1991).

There is a region of high topography in the southeast corner of Milna, where the inlet valley terminates. We interpret this as a spatial concentration of sediment deposited into Milna as the result of focused deposition from a river within the inlet valley as that river debouched into Milna. The maximum elevation of this large southeast sedimentary deposit is ~280 m, which is approximately the same elevation as the floor of the outlet valley (Fig. 2). The timing of fluvial activity through the secondary inlet (Fig. 2) relative to the timing of fluvial activity through the main inlet cannot be well constrained, but the secondary inlet becomes unconfined by valley walls at a valley floor elevation of ~290 m,

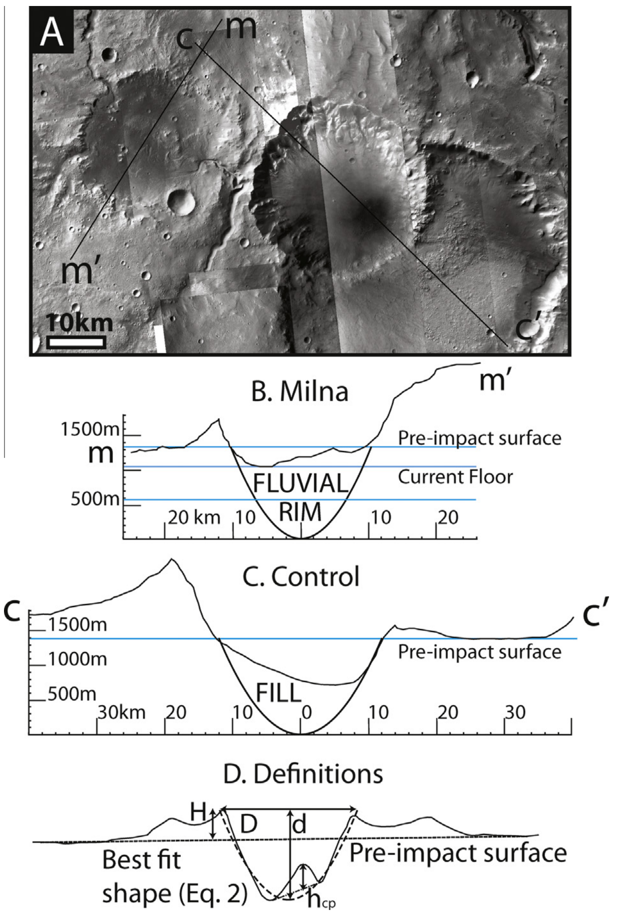

Fig. 3. (A) Milna Crater and the adjacent control crater; MOLA topographic profiles using 1/128 pixel per degree gridded data were taken along the black lines (B and C). (B) A topographic profile with 10× vertical exaggeration along the line from m to m′ is superimposed over the crater profile obtained from Eq. (2) (also 10× vertical exaggeration) based on a 20% smaller 'pre-backwasting' diameter (22.5 km, see Section 5.1). Vertical scale is given relative to the calculated initial base of the fresh crater. The assumed pre-impact surface, 280 m above the current lowest point in Milna, as well as the elevation of the current lowest point in Milna are given. The depth to which rim material was estimated to fill Milna (Eq. (13)) is also given 'RIM.' 'FLUVIAL' is the cross-sectional slice of the volume of fluvial fill bounded by the elevation to which rim material filled the crater and the current topography. (C) Same as (B), but with the topographic profile taken along the line from c to c′, over the control crater, which is assumed to have backwasted 20% as well (note prominent alcoves on the north rim of the control crater), giving an initial crater diameter of 25 km, and with an assumed pre-impact surface of −260 m (see Section 5.4). (D) Definitions of H (rim height), D (diameter), d (depth), h_{cp} (central peak height), and best fit cavity shape (Eq. (2)). Adapted from Garvin et al. (2000). *Image is CTX (P01_001586_1563, P14_006465_1582), THEMIS VIS (V19060005, V16614006, V16302005); profiles from MOLA.*

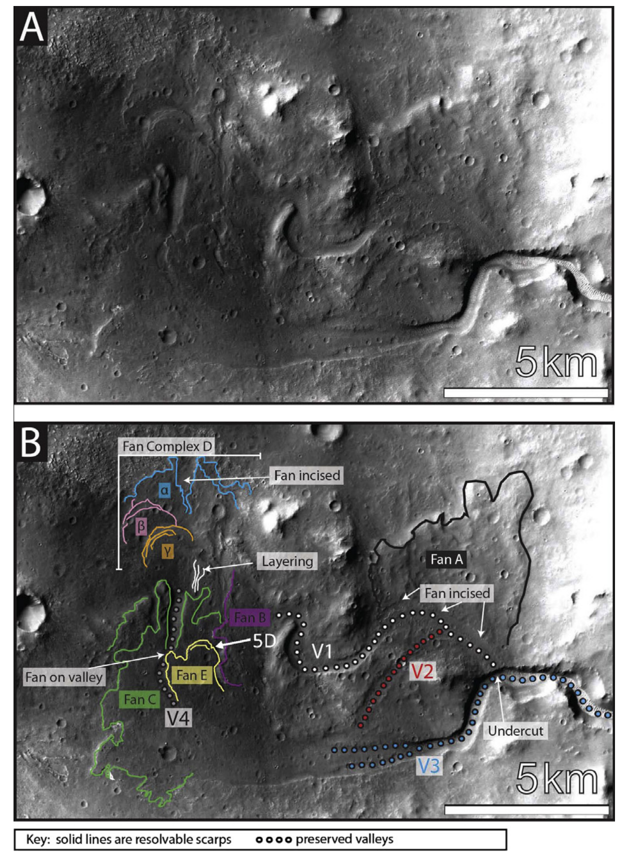

Fig. 4. (A) There is a large fan with several lobes that are incised by sinuous valleys in the southeast corner of Milna just below the inlet valley. Note the dunes obscuring the floor of the inlet valley (bottom right). (B) An annotation of (A), which is thoroughly described in Section 3.3. Note the fan that superposes a valley, the incision of previously deposited fans in several locations, and that the valleys are sinuous and branched. Note also the stacked scarps visible at this (CTX) resolution in Fan Complex D, and Fans C and E. There are also stacked scarps in the dissected area west of Fan B not associated with a discrete lobe. The location of figure 5D is also indicated. *Image is CTX (P01_001586_1563), THEMIS VIS (V16302005).*

similar to the elevations of the outlet valley floor and the top of the southeast sedimentary deposit.

Much of this sedimentary deposit does not record identifiable, spatially discrete deposition lobes. However, there are five regions that we identify as depositional fans because of their generally lobate shape and steep scarp margin, and some of these have multiple lobes (Fig. 4). The following observations and interpretations are based mainly on the information conveyed in Fig. 4.

Fan A is ~50 m thick and its top surface is located at ~280 m. Fan A is incised by Valley V1, which terminates at the top surface of Fan B (~180 m). Fan B is heavily eroded along its western margin; to the west of Fan B there is a region of exposed stacked scarps that are not definitively related to any spatially distinct lobe. We therefore interpret that Fan A was deposited before incision by V1, and that V1 contained a river that carried sediment that was deposited to form Fan B.

There is a node where V1 and Valley V2 branch. This node is located downslope from a point at which Valley V3 undercuts the valley that is the common trunk of V1 and V2. We thus interpret that there was a river leading from the inlet valley that avulsed and pirated water away from V1 and V2, into V3, and that the formation of V3 postdates both V1 and V2. However, it is impossible to determine whether the formation of V1 predates, postdates, or was contemporaneous with the formation of V2.

V3 furcates to the west, in the direction of lower topography. Fan C is approximately 10 km from where the inlet valley enters Milna and has a top surface elevation of ~180 m. Valley V4 incises Fan C. We group Lobes α, β, and γ into Fan Complex D because of their stacked spatial relationship; Lobe α has a top surface elevation at ~70 m, Lobe β at ~90 m, and Lobe γ at ~130 m. Fan E drapes onto V4, which indicates that Fan E must have formed after V4.

We interpret that fluid flowing through V3 (as opposed to V1, which terminates at and does not incise into Fan B, or V2, which is truncated by V3) brought sediment to Fans C–E after the formation of Fan A and Fan B. However, the margin between the scarps of Fan B and Fan C are not preserved well enough to clearly determine whether (i) Fan C abuts the scarp of Fan B, or whether (ii) Fan B sits partially on top of Fan C. In the second scenario (ii), it is also plausible that a proto-V3 was active at the same time as V1 and thus that the formation of portions of Fan C are contemporaneous with, or even younger than, the formation of Fans A–B. Nevertheless, Fan

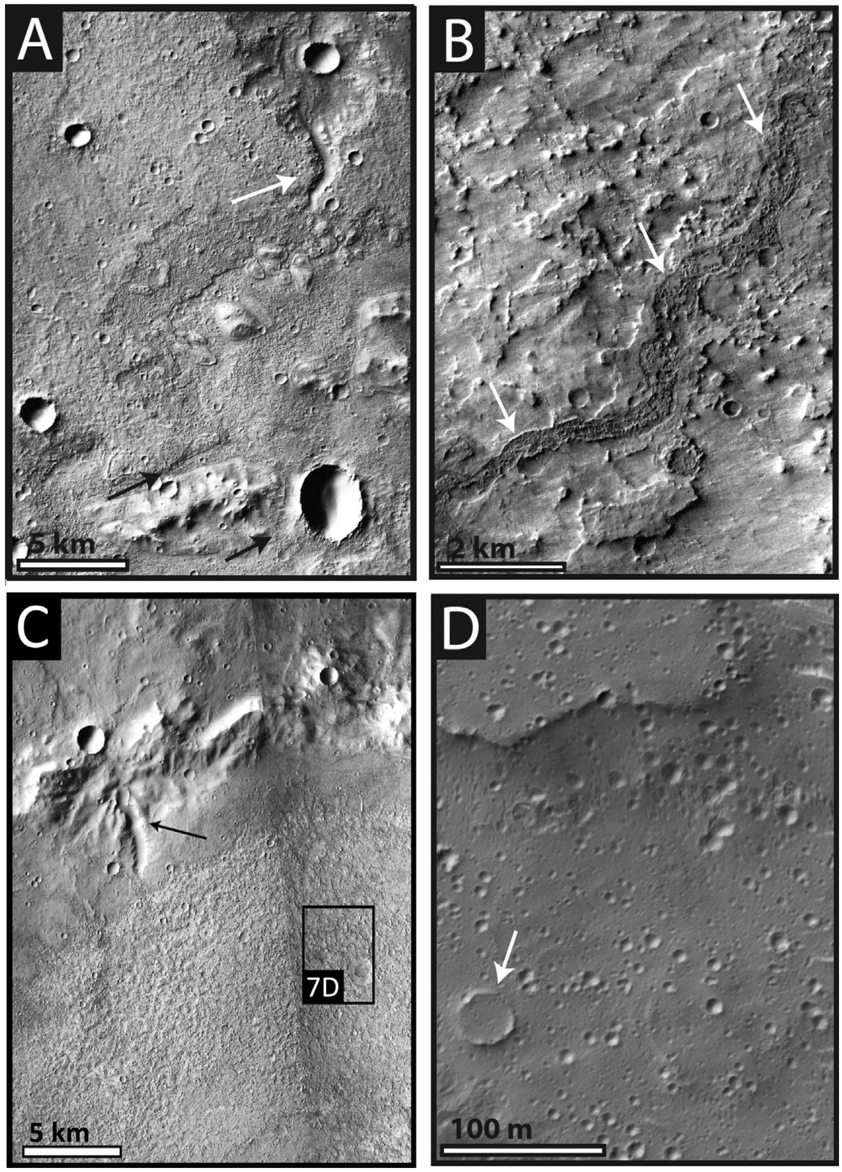

Fig. 5. (A) The southern basin. Note the channel leading to the broad valley (white arrow) and the two short valleys sloping into the depression (black arrows). (B) The outlet valley from Milna becomes an inverted channel with a hummocky texture. (C) The prominent impact crater at the bottom center of the drainage area sourcing Milna (Fig. 6) has a cluster of small valleys that allow draining into the rest of the drainage area. Context for Fig. 7D is given. (D) Inverted craters in the interior of Milna. *Image is (A and C) CTX (P01_001586_1563), (B and D) CTX (P14_006465_1582).*

Table 2
Volumes of craters and fill. The original and filled-in volumes of Milna Crater and the control crater (Fig. 3) are given, assuming either that the crater radius has expanded 20% due to backwasting or has not (see Section 5.1). The difference between the current (filled) volume and the original volume is given as the volume of fill.

Feature	Volume (no backwasting, km^3)	Volume (backwasting, km^3)
Milna original	316	195
Milna filled	50	50
Milna volume of fill	266	145
Control original	419	232
Control filled	187	187
Control volume of fill	232	45

C was deposited before Fans D–E because V4 incises Fan C but does not continue to the north and incise Fan Complex D.

In Fan Complex D we interpret that Lobe α was deposited before Lobe β, which was deposited before Lobe γ, because of their elevation relationships. We interpret that the sediment in Fan Complex D was delivered through a channel in V4. Lobe α is incised by a valley that rapidly widens, which may suggest that the valley was formed by a channel that incised the lobe when the sediment was not yet lithified. Lobe β and Lobe γ are stepped fans, which can indicate rising water conditions as they were deposited (De Villiers et al., 2013; although steps in fans can also indicate changes in water or sediment supply, changes in wave activity in the basin, or erosion of the fan long after it was formed).

Finally, we interpret that Fan E records the last pulse of fluvial sediment transport capable of depositing a fan because it drapes onto V4 and no other valleys or fans within Milna appear to postdate Fan E. In addition, some exposed stacked scarps in the region just west of Fan B indicates that there are layered deposits under Fans A–E. This indicates that Fans A–E were deposited in the last stages of fluvial activity in Milna, but that there may have been other fans that are now covered.

Since the elevation of Fan A corresponds well with the current outlet valley elevation (Fig. 2A), it is likely that Milna was as an open basin lake during the deposition of Fan A. However, the valleys leading to the other fans are significantly below the outlet valley elevation (Fig. 2A). Our favored hypothesis is that at some time between the deposition of Fan A and Lobes β and γ the water surface level dropped below ~70 m (the surface elevation of Lobe α), possibly completely drying out, before rising again.

4. Timescale estimation techniques

To estimate the timescale for which there was active fluvial sedimentary deposition in Milna, we calculate the time to fill the crater with its current volume of sediment. Although the fill in the crater need not be entirely deposited as a result of fluvial activity, we focus on fluvial sedimentation timescales in this section, and address the role of other potential sources of fill in Section 5. Quantitative timescale results for Milna are presented in Section 6.

We assume that the sediment is not supply limited; that is, the source region always has enough sediment to allow the sediment fluxes predicted by our model. We make this assumption on the basis that a ~1–2 km depth of megaregolith (breccias formed by impacts, representing a mobile sediment source) would have been available for transport (e.g. Wilson and Head, 1994) from the sourcing drainage area (Fig. 6).

4.1. Initial crater dimensions

In order to find the volume of the crater, the curve describing the shape of the crater cavity is integrated as a solid of rotation. To describe the shape of the crater, the depth of the crater, d, must be calculated using the diameter of the crater, D (Garvin et al., 2002):

$$d = 0.36D^{0.49} \tag{1}$$

The shape is then described by (Garvin et al., 2002):

$$z(x) = bx^{0.81D^{0.28}} \tag{2}$$

where $z(x)$ is the vertical dimension inside the crater, x is the horizontal dimension of the crater extending from the center of the crater, and b is a shape fitting parameter. The shape fitting

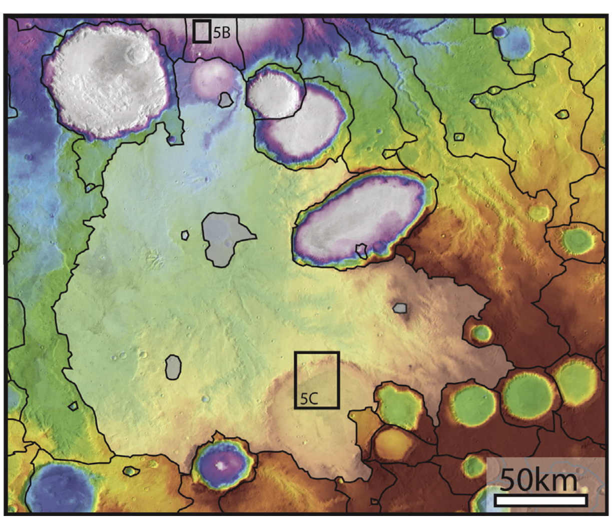

Fig. 6. The drainage area leading to Milna Crater is 3.5×10^4 km^2 (translucent white). All of the excluded regions within the drainage area (gray), except the largest, are probably due to impacts that happened after the period of heavy fluvial modification around Milna. The prominent impact crater at the bottom center of the drainage area sourcing Milna has been extensively filled in and is breached by a cluster of valleys that flows into the rest of the drainage area sourcing Milna (Fig. 5C). Context is given for Fig. 5B and C. The elevation gradient derived from MOLA is given, scale: [0 m, white, to 2000 m, red]. *Basin divides generated from MOLA 1/128 pixel per degree gridded data; background is a THEMIS IR mosaic.* (For interpretation of the references to color in this figure legend, the reader is referred to the web version of this article.)

parameter b can be determined by noting that $z\ (x = \frac{D}{2})$ must equal the depth of the crater.

To calculate the volume of the crater, a reference surface must be used. Noticing that crater depth is defined with respect to the rim height, H, the pre-impact surface corresponds to the difference between depth and rim height and is a convenient reference surface (see Fig. 3). The rim height is given by (Garvin et al., 2002):

$$H = 0.05D^{0.60} \tag{3}$$

Using the crater depth, shape profile, and rim height, the volume (V_0) of a fresh crater (excluding the central peak) below the pre-impact surface can be found by:

$$V_0 = 2\pi \int_0^{D/2} x(d - (H + z))dx \tag{4}$$

Note that Eqs. (1)–(4) use units of kilometers.

4.2. Sediment fill and flux

Once the original cavity volume (V_0) is known, then the amount of sedimentary fill (V_S) is calculated by subtracting the current volume of the crater cavity (V_C) from the original fresh volume of the crater cavity, after taking into account the porosity (φ, assumed to be 0.31 throughout this paper, see Mavko et al., 2009) of the deposited sediment:

$$V_S = (1 - \varphi)(V_0 - V_C) \tag{5}$$

The timescale T to build the sedimentary fill in the crater is the volume of sedimentary fill divided by the sediment flux. The total sediment flux comprises bedload flux (Φ) and suspended sediment flux, where k denotes the suspended-to-bedload transport ratio, which yields a calculation of the timescale:

$$T = \frac{V_s}{\Phi(k+1)} \tag{6}$$

The suspended-to-bedload transport ratio is estimated by using values obtained on Earth, which range from ~1 to greater than 10 (e.g. Duck and McManus, 1994; Pratt-Sitaula et al., 2007; Turowski et al., 2010); this is discussed further in Section 6.4.

The volumetric bedload flux Φ is determined using the equation derived by Fernandez Luque and Van Beek (1976), in which the quantity τ_*, the Shields stress (the basal shear stress normalized by the submerged grain weight per unit area), must be greater than 0.045 for bedload flux to occur:

$$\Phi = 5.7W\left[g\left(\frac{\rho_s - \rho_f}{\rho_f}\right)D_S^3\right]^{1/2}[(\tau_* - 0.045)^{3/2}] \tag{7}$$

$$\tau_* = \frac{hS}{D_S(\rho_s - \rho_f)/\rho_f} \tag{8}$$

Eqs. (7) and (8) depend on the width of the channel (W), the slope of the channel (S), gravity (g), the sediment density (ρ_S), the fluid density (ρ_f), the sediment diameter (D_S), and the depth of fluid in the channel (h). The values we use for these inputs are summarized in Table 3.

4.3. Channel dimensions

Even though the valley dimensions in Milna can be clearly measured, the channel dimensions cannot. It is imperative to understand how the size of martian valleys reflects their potential for fluid transport. The difficulty in this assessment stems from the fact that many valleys on Mars date back to ca. the Noachian–Hesperian boundary (e.g. Fassett and Head, 2008a), and have thus

Table 3
Effects of channel type. The variables and assumptions used for each type of channel bed. Width–depth ratio: depth of fluid in a channel as a fraction of channel width (see Schumm and Khan, 1972; Finnegan et al., 2005). D_S: sediment diameter used to calculate the Darcy–Weisbach coefficient of crater friction (see Wilson et al., 2004), log is the base-ten logarithm; values of D_S are given in Table 5. Equations for $(8/f_c)^{1/2}$ come from Wilson et al. (2004), r is the element roughness scale for a channel with a fixed bed. Measured and assumed variables for the constants given in Section 4.1 are also listed.

Type	Width–depth ratio	D_S	$(8/f_c)^{1/2}$
Sand	1.2%	Use D_{50}	$8.46(R/D_S)^{.1005}$
Gravel	1.7%	Use D_{84}	$5.75\log(R/D_S) + 4.0$
Bedrock	20.0%	.12–.50 m	$5.657\log(R/r) + 6.6303$
Assumed/measured variables			
Sed. density	2800 kg m^{-3}	Gravity	3.71 m s^{-2}
Fluid density	1000 kg m^{-3}		

been subject to billions of years of aeolian erosion. Even at the slow erosion rates measured for Mars (e.g. Golombek et al., 2006), resolvable signs of ten-meter to hundred-meter scale inner channels can be erased (see Craddock and Howard, 2002). This problem is compounded by the pervasiveness of dunes that accumulate in martian valleys, further obscuring the morphology of valley floors (e.g. Fig. 4). Additionally, many terrestrial valleys contain channels that are smaller than their host valley, such as the particularly striking example of the Grand Canyon in the western United States.

Although simply equating valley geometry to channel geometry is inappropriate (see Wilson et al., 2004), Penido et al. (2013) have found that valley width is a valid indicator of channel width. We conducted an independent survey of inner channels within the Margaritifer Sinus Quadrangle (0S, 0W to 30S, 45W), which contains some of the inner channels identified by Irwin et al. (2005a). We find that the average ratio of channel to valley width, with one standard deviation, is 0.18 ± 0.08 (Table 4), which is similar to the ratios obtained by Penido et al. (2013) for inner channels derived from measurements over many locations on Mars.

Finally, the resolution at which topography can currently be measured from orbit is not high enough to determine the depths of inner channels, and the presence of sand dunes in many of these channels stymies attempts even as higher resolution images become available. Thus, we use channel depth-to-width ratios derived from terrestrial observations to estimate channel depths (Table 3; Schumm and Khan, 1972; Finnegan et al., 2005).

4.4. Sediment diameter

The sediment size distribution is not well constrained at Milna, which makes flux estimates difficult (e.g. Kleinhans, 2005). We thus calculate bedload sediment flux using a range of potential sediment diameters: 1.2–12 cm, the D_{84} estimated from the sediment distributions at Gale Crater and Ares Vallis, respectively, spanning the entire range of sediment distributions known from Mars so far (Golombek et al., 2003; Wilson et al., 2004; Williams et al., 2013; see Table 5). The Ares Vallis distribution likely represents material moved in discharges much larger than those that would have entered Milna (cf. fluxes calculated by Komatsu and Baker, 1997) and thus represents a reasonable maximum value. HiRISE images definitively constrain the upper bound, because blocks of half-meter diameter and larger (the limit of resolution) are not observed in fan scarps.

To confirm that sediment is in bedload as sediment diameter is varied, we calculate the shear velocity u^*:

$$u^* = \sqrt{ghS} \tag{9}$$

We also calculate the terminal settling velocity w_S (Ferguson and Church, 2004):

$$w_S = \frac{R_s g D_s^2}{C_1 \nu + (0.75 C_2 R_s g D_s^3)^{0.5}} \tag{10}$$

where R_s is the submerged specific gravity of the sediment, ν is the kinematic viscosity of the fluid (we use a range of ν from 1.8×10^{-6}

Table 4
Channel to valley ratios in Margaritifer Sinus Quadrangle. Results from a survey of inner channels within Margaritifer Sinus Quadrant (0–30S, 0–60W), which includes three channels mapped by Irwin et al. (2005a). The location of the inner channels is given, along with the image in which they were identified. The valley and channel widths are the mean of 15 evenly spaced measurements perpendicular to the valley walls (for valley widths) or channel walls (for channel widths) along the resolvable inner channel for the length given in the 'section length' column. Ratio: the channel width divided by the valley width.

Location	Image	Channel width (m)	Valley width (m)	Ratio	Section length (km)
Survey within Margaritifer Sinus Quadrangle					
10.17W, 23.66S	P03_002285_1562 (CTX)	180	1650	0.11	0.9
19.30W, 23.60S	B01_010091_1541 (CTX)	566	2071	0.27	5
19.80W, 22.15S	E2300216 (MOC)	808	2417	0.33	15
19.87W, 21.70S	E2300216 (MOC)	995	2741	0.36	20
19.88W, 22.21S	P07_003894_1562 (CTX)	347	2028	0.17	15
21.31W, 19.43S	P17_007731_1589 (CTX)	721	2398	0.30	10
21.63W, 18.81S	P02_001982_1611 (CTX)	548	1899	0.29	4
22.92W, 23.22S	B12_014403_1576 (CTX)	243	1754	0.14	10
22.94W, 23.30S	B12_014403_1576 (CTX)	190	1817	0.10	10
23.00W, 23.43S	B12_014403_1576 (CTX)	148	1704	0.09	10
25.26W, 26.78S	P18_008074_1536 (CTX)	503	2242	0.22	10
25.66W, 26.62S	P18_008074_1536 (CTX)	453	2229	0.20	5
30.21W, 20.02S	P05_003090_1578 (CTX)	27	200	0.14	4
30.22W, 23.33S	P05_003090_1578 (CTX)	91	423	0.22	2.5
30.24W, 23.02S	P05_003090_1578 (CTX)	27	281	0.10	1.6
30.27W, 23.04S	P05_003090_1578 (CTX)	33	216	0.15	4
31.88W, 26.57S	B01_009986_1534 (CTX)	58	584	0.10	15
32.93W, 25.64S	P19_008272_1545 (CTX)	34	370	0.09	2
32.94W, 25.66S	P19_008272_1545 (CTX)	38	326	0.12	4
33.06W, 24.99S	P19_008272_1545 (CTX)	51	397	0.13	1.2
33.94W, 24.04S	B02_010408_1548 (CTX)	134	605	0.22	15
Reported by Irwin et al. (2005a)					
14.63W, 9.56S	P04_002496_1686 (CTX)	651	4317	0.15	15
9.91W, 24.17S	P02_002008_1558 (CTX)	228	1420	0.16	8
2.44W, 22.41S	V01686002 (THEMIS)	275	2450	0.11	10

Mean: 0.18, standard deviation: 0.08, interquartile range: 0.11–0.22.

Table 5
Sediment characteristics. Sediment distributions from Ares Vallis (Golombek et al., 2003; Wilson et al., 2004) and Gale Crater (Williams et al., 2013). Sand distributions are also given from Meridiani Planum (Grotzinger and Athena Science Team, 2004) and Gusev Crater (Herkenhoff et al., 2004); see also the table in Kleinhans (2005).

Location	D_{50} (m)	D_{84} (m)	D_{90} (m)
Gravel			
Ares Vallis	0.05	0.12	0.16
Gale Crater	0.0044–0.0095	0.0065–0.018	
Sand			
Meridiani Planum	0.0004		0.0008
Gusev Crater	0.0014		0.0017

to 8.0×10^{-7}, corresponding to a temperature range of 0–30 °C), and C_1 and C_2 are constants that represent grain shape (C_1 = 18–24 and C_2 = 0.4–1.2, a range from smooth spheres to natural particles, Ferguson and Church, 2004). We then compare u^* and w_S each time that the bedload flux is calculated. Sediment in the 1.2–12 cm size range is always in bedload over the entire range of channel geometries investigated. However, the sediment size distribution has been found to be bimodal at the martian landing sites (e.g. discussion in Kleinhans, 2005), so there is a significant proportion of sand in addition to the larger sediment just discussed, with sand diameters ranging from ~0.1 to 1.7 mm; these diameters are estimated from the distributions found at Meridiani Planum and Gusev Grater (Grotzinger and Athena Science Team, 2004; Herkenhoff et al., 2004; see Table 5).

We find that for all channel dimensions considered in this paper, over the entire range of grain shapes and kinematic viscosities, that sediment in the sand size range (~0.1–1.7 mm) is always carried in the suspended load. The sand is accounted for by using k, the suspended-to-bedload transport ratio (Section 4.2).

4.5. Fluid filling timescales

The time, T_{min}, to flood a fresh crater cavity with fluid, the minimum condition required to form an outlet valley (e.g. Fassett and Head, 2008b), can also be calculated (cf. discussions in Matsubara and Howard, 2009; Matsubara et al., 2011). To do this, the fluid flux, Q, must be calculated, which relies on the mean fluid velocity in the channel, U:

$$Q = UWh \tag{11}$$

$$U = \sqrt{8gRS/f_c} \tag{12}$$

We make use of the Darcy–Weisbach equation to calculate the mean fluid velocity, as recommended by Komar (1979) and Wilson et al. (2004) (see also the discussion by Kleinhans, 2005). We determine the Darcy–Weisbach friction factor (f_c) using the treatment described in Wilson et al. (2004), which adapts the equations of Bathurst (1993) under terrestrial conditions to use under martian conditions (see channel-type dependent values for f_c in Table 3). The hydraulic radius of the channel (R) is determined from our calculations of channel dimensions (Section 4.2). T_{min} is calculated by dividing the cavity volume by the fluid flux through the inlet channel. The timescales calculated for flooding Milna are always at least two orders of magnitude smaller than the timescales needed to construct the sedimentary fill under the same conditions (see Table 6).

5. Non-fluvial sources of crater modification

There are several potential sources of fill in Milna, not just from fluvial transport. Additionally, post-impact modification can change the geometry of the crater, including its diameter (e.g. Forsberg-Taylor et al., 2004). These processes complicate calculating timescales of fluvial sediment emplacement into Milna.

5.1. Backwasting

While backwasting adds no net fill to the crater, it does expand the diameter of the crater, complicating the estimate of the original volume of the crater and thus also the estimate of the volume of sedimentary infill. Highly degraded craters, such as Milna, can have their diameters increased by as much as 20% (Fig. 3; Forsberg-Taylor et al., 2004). If the diameter of Milna has increased 20% compared to its original diameter, then the original crater diameter would be approximately 22.5 km; this is also consistent with the observation that the outlet valley incises fill material for several kilometers before exiting the crater (Fig. 2D). This scenario requires less fill to achieve the current topography seen in Milna. If one assumes no backwasting has occurred (a poor assumption), Milna has been filled with 266 km^3 of sediment; however, assuming the diameter has been increased by 20%, Milna has been filled with 145 km^3 of sediment (see Table 2).

5.2. Rim erosion

We estimate the amount of fill due to rim erosion by calculating the depth of a crater that has been filled in with eroded rim material (d_{rm}) (derived from Craddock et al., 1997):

$$d_{rm} = 0.71(0.072D^{.792}) \tag{13}$$

The difference between the depth of the fresh crater (Eq. (1)) and the filled in crater yields the depth of the fill material obtained from rim erosion alone. For Milna, this is a depth of 570 m of fill. Then, applying appropriate bounds to Eq. (4) yields the volume of the solid of rotation of the fill material due to rim erosion. For Milna, this is 37.6 km^3, or 19% of the original volume of the cavity, assuming that the original crater diameter was 22.5 km.

5.3. Other fill sources

Several other sources of fill could contribute to the sedimentary volume in Milna, in addition to fluvial transport and rim erosion. The volume taken up by the central peak, volcanic surface flow, volcanic ash-fall, aeolian transport, and ejecta from younger craters could all add to the fill volume (e.g. discussion in Forsberg-Taylor et al., 2004). However, thermal or volumetric expansion of sediment or the crater walls are unlikely to significantly impact the amount of fill calculated for Milna Crater (see discussion in Craddock et al., 1997).

The volume of the central peak was calculated as a cone with central peak height and central peak diameter calculated from the equations found in Garvin et al. (2003). In Milna, the central peak volume accounts for approximately 2 km^3 (1%) of the volume of fill needed to create the current topography, assuming that the original crater diameter was 22.5 km. Significant volcanic ash-fall, ejecta, and aeolian contributions after the fluvial emplacement of the fans are inconsistent with the deflational post-emplacement modification of the fans and inverted morphologies observed in Milna (Figs. 4 and 5; discussion in Williams et al., 2009).

5.4. Test of assumptions of non-fluvial fill

As a further test to determine a plausible amount of non-fluvial crater fill, we measured the amount of fill in an adjacent, 30 km diameter crater (labeled ‘Control’ in Fig. 3). The drainage area surrounding the control crater is essentially limited to the crater perimeter itself, and there are no channels entering into the control crater. We thus assume that all of the fill in the control crater is due to non-fluvial sources. Since the inlet valley to Milna is not disrupted by this adjacent crater, we assume that this crater impacted prior to the fluvial activity in Milna. Although precise constraints on the age relationship between Milna and the adjacent control crater are not possible, the fill in the adjacent control crater still acts as a useful test of our assumptions for non-fluvial fill.

The initial volume of the control crater was calculated as prescribed in Section 4.1. Due to the heavily modified rim (see Fig. 3) we assume that the crater has also experienced 20% enlargement due to backwasting, and so the initial volume is calculated assuming an original crater diameter of 25 km. The impact that created the control crater hit partially into an older crater, complicating the geometry (see Fig. 3). However, to calculate the maximum possible fill in the control crater, we use the lowest elevation in the surrounding topography (−260 m, see Fig. 3) to constrain the current volume of the control crater. We calculate an initial volume of 232 km^3 (see Section 4.1) and measure the current volume as 187 km^3, which means that the volume of fill is 45 km^3, or 19% filled. The value of 19% fill is commensurate with the volumes we calculate based on eroded rim material and central peak volume combined in Milna (20%), with negligible additional non-fluvial fill. We thus proceed assuming 20% non-fluvial fill in Milna Crater.

5.5. Fluvial transport

Based on the numerous, discrete fans and sinuous valleys in Milna (Fig. 4), and our calculations of non-fluvial fill, fluvial transport likely accounts for the other 80% of the fill in the crater. The spatial distribution of sediment also indicates extensive fluvial deposition because the fill in Milna is built up preferentially near the inlet valley (Fig. 2). The total volume of fill in Milna is 145 km^3, which yields 20 km^3 of non-fluvial sediment and 80 km^3 of fluvially derived sediment (after taking an assumed porosity of 0.31 into account), assuming that the diameter of Milna has been enlarged by 20%. Fluvial erosion of the inlet valley accounts for 4 km^3 of fill, meaning that the remaining fluvially transported sediment budget (76 km^3) comes from the erosion of the surrounding drainage area. The drainage area around Milna is 3.5×10^4 km^2 (Fig. 6).

6. Timescale results for Milna Crater

Using the geometry of the inlet valley, the minimum and maximum timescales for the formation of the fluvial sedimentary fill can be estimated under the assumption of continuous flow and sediment transport (Sections 6.1 and 6.2). These estimates are improved by a comparison to a calculation of fluid flux through the outlet channel (Section 6.3) and then incorporated to construct a preferred hypothesis for the timescale to deposit the fluvial fill in Milna (Section 6.4). To perform these calculations, we assume that the walls of the inlet channel are composed of gravel because the flow rates estimated through the inlet channel entrain all sand particles into suspended flux (see Section 4.3) and a bedrock channel is incompatible with our assumption of non-limited sediment supply (see Section 4). The choice of a gravel bed is consistent with the grain-size distribution we assume.

6.1. Minimum timescale from inlet channel flow

The absolute minimum timescale is calculated assuming the sediment size is as small as possible (though still remaining in bedload, see Section 4.3, Eq. (6)) because our model predicts that sediment flux is higher when composed of particles of smaller diameter. Thus we choose the sediment size distribution with the smallest D_{84} diameter that remained in bedload, 2.2 cm (slightly larger than values from Gale Crater, Williams et al., 2013, Table 5). We assume a channel width of 250 m because that is the width of the narrowest portion of the inlet valley (Fig. 2). Since the average width of the inlet valley for Milna is 1100 m, this ratio is 0.23, within one standard deviation of the ratio we

Table 6

Timescale results and input values. Numerical results of timescale estimations based on flux through the inlet channel, listed with variable value choices (see Section 6). Preferred and alternate timing scenarios are discussed in Section 6. Sediment sizes for gravel channel model runs were selected based on values given in Table 5; D_S = 0.5 m, r = 1 m were chosen for bedrock because these are the largest values possible, as constrained by HiRISE imagery. Channel:valley is the ratio of the channel width to the valley width. Suspension:bedload is the ratio of suspended sediment to bedload sediment flux. Crater size: the increase in diameter due to weathering (see Forsberg-Taylor et al., 2004). Non-fluvial fill: the percentage of fill from non-fluvial sources. Fluvial fill: the remaining fill not attributed to non-fluvial sources. Channel type: encapsulates the assumptions, including Darcy–Weisbach friction factor and width-to-depth ratios, in Table 3. Timescale: the numerical result for timescales of continuous flow required to construct the fluvial fill in Milna. Numerical results for fluid flux and sediment flux through the channel are given. The total water volume needed to accomplish total sediment transport is also given. Sed. conc. = sediment concentration in the fluid. Finally, the thickness of eroded material from the drainage area required to build the fluvial fill in the crater, the rate at which that material would have been eroded given the calculated timescales of continuous flow, and timescales to flood the crater with water for both the current geometry and the calculated original geometry are given.

	Minimum timing	Maximum timing	Preferred timing
Variables	*Value*	*Value*	*Value*
Channel:valley	0.23	0.09	0.15–0.23
Valley width (m)	1100	1100	1100
Slope	0.011	0.011	0.011
Suspension:bedload	10:1 ratio	1:1 ratio	1.25:1 ratio
Crater size	20% expansion	No expansion	20% expansion
Porosity	0.31	0.31	0.31
Non-fluvial fill	20%	20%	20%
Fluvial fill (km^3)	80	147	80
Channel type	Gravel	Gravel	Gravel
Sediment size (cm)	2.2	12	2.2–12
Timescale (yr)	15	4700	75–365
Fluid flux ($m^3\ s^{-1}$)	7.4×10^3	4.3×10^2	$1.7–7.4 \times 10^3$
Sed. flux ($m^3\ s^{-1}$)	1.7×10^2	1.0×10^0	$7.0 \times 10^0–3.4 \times 10^1$
Total water (m^3)	3.6×10^{12}	6.4×10^{13}	$1.8–2.0 \times 10^{13}$
Sed. conc. ($g\ l^{-1}$)	62	6	11–13
Eroded material (m)	2.2	4.2	2.2
Erosion rate (m/yr)	1.5×10^{-1}	9.1×10^{-4}	$6 \times 10^{-3}–2.9 \times 10^{-2}$
Water flooding timescale			
Fresh geometry (yr)	0.83	23	0.83–3.6
Current geometry (yr)	0.21	3.7	0.21–0.91

measured from our survey of the Margaritifer Sinus Quadrangle (Table 4). We assume a high suspended-to-bedload sediment flux ratio of 10:1 so that the total flux is maximized (Table 6). We assume that the original crater diameter has been expanded by 20% (cf. Forsberg-Taylor et al., 2004) and that non-fluvial sources account for 20% of the sedimentary fill (see Section 5).

Using these assumptions and Eqs. (5)–(12) means that 80 km^3 of the fill is attributed to fluvially transported sediment and that the sediment flux is 1.7×10^2 m^3 s^{-1}. This gives a minimum timescale of 15 terrestrial years for continuous fluvial deposition of sediment and requires 2.2 m of erosion averaged over the drainage area (Fig. 6; Table 6).

6.2. Maximum timescale

The absolute maximum timescale is calculated assuming the sediment size is large because our model predicts that sedimentary flux is lower when composed of particles of larger diameter. We therefore assume the grain-size distribution from the Ares Vallis landing site, with D_{84} of 12 cm, which has the largest reported grain-size distribution of the martian landing sites that are interpreted to record fluvial modification (see Golombek et al., 2003; Wilson et al., 2004; Williams et al., 2013). We assume a channel-to-valley ratio of 0.09 because this is the smallest ratio we measured in the Margaritifer Sinus Quadrangle (Table 4). We assume a low suspended-to-bedload sediment flux ratio of 1:1 so that the total flux is minimized. We assume that the original crater diameter has not been expanded and that non-fluvial sources account for 20% of the sedimentary fill (see Section 5).

Using these assumptions and Eqs. (5)–(12) means that 147 km^3 of the fill is attributed to fluvially transported sediment and that the sediment flux is 1.0 m^3 s^{-1}. This gives a maximum timescale of 4.7×10^3 terrestrial years for active fluvial deposition and requires 4.2 m of erosion averaged over the drainage area (Fig. 6; Table 6).

6.3. Comparison of inlet and outlet channel flow

The outlet channel of Milna continues northward, leading to a kilometers-long, sinuous ridge with a hummocky texture, which we interpret as an inverted channel formed by flowing water (cf. Williams et al., 2009; Fig. 5B). The presence of an inverted channel affords another opportunity to check the sediment transport conditions by placing independent constraints on the fluid flux through the system. The inverted channel has km-length regions where its edges are parallel or sub-parallel, and other regions where the planform of the ridge bulges outward. We measure the width of the inverted channel along the regions where the edges are approximately parallel and find that the width of the channel ranges between 280 and 320 m wide. We assume that this width corresponds to the bankfull width of the channel at which maximum work on the landscape was accomplished; i.e. at the discharge that, over time, is most effective at redistributing sediment (cf. Wolman and Miller, 1960). We also measure that the slope of the inverted channel is 0.005, and we assume that this is representative of the slope of the channel when it formed. Note, though, that estimation of width and slope of an inverted channel can be complicated both by depositional effects, e.g. channel migration leaving a wider channel body deposit than the true width of the channel, and post-depositional effects, e.g. narrowing of the inverted channel by erosion (see DiBiase et al., 2013).

Given these measurements of slope and width, and using Eqs. (12)–(14), we can calculate a range of fluid fluxes through the channel, assuming a channel with gravel banks. To calculate the maximum spread in fluid flux, we use a large grain size (12 cm) for the narrow channel (280 m) and a small grain size (1.3 cm, the smallest that remains in bedload) for the wide channel (320 m). We find that fluid fluxes between 4.9×10^3 and 9.4×10^3 m^3 s^{-1} correspond to the bankfull flux through this channel (see Table 7). Noting the discussion in Kleinhans (2005), we assume an error of approximately a factor of three when using the Darcy–Weisbach equation and thus have a preference for scenarios in which flux through the inlet valley is between $\sim 2 \times 10^3$ and $\sim 3 \times 10^4$ m^3 s^{-1}. This range of fluid fluxes is also compatible with the results when fluxes are calculated using the values of the valleys incised into the fan deposits (S = 0.0067, W = 250 m), which should record the true typical width of the channel when most of the sediment is transported (Wolman and Miller, 1960).

6.4. Preferred hypothesis

Given the discussion in the previous subsection, we describe our preferred hypothesis. The assumptions are summarized in Tables 3, 5, and 6. Following the discussion in Section 5, we assume that the crater diameter has been 20% enlarged (cf. Forsberg-Taylor et al., 2004).

We favor a gravel channel with a channel-to-valley ratio of 0.15–0.23, which gives fluxes commensurate with the flux calculated for the outlet valley and the valleys incising into the fan complex (namely, between $\sim 2 \times 10^3$ and $\sim 3 \times 10^4$ m^3 s^{-1}; see Section 6.3), and is near the mean channel-to-valley ratio in the Margaritifer Sinus Quadrangle (Table 4). Gravel is also a bed texture compatible with the grain-size distributions spanning from Gale Crater to Ares Vallis and the sediment size we assume (Section 4.4).

Several authors have found that during flood conditions or when averaged over long time periods, the terrestrial suspension-to-bedload ratio is about 1.25:1 (Duck and McManus, 1994; Pratt-Sitaula et al., 2007; Turowski et al., 2010). Thus we assume a suspension-to-bedload ratio of 1.25:1, which gives compatible calculations of suspended sediment load as compared to those measured in terrestrial rivers in arid and semi-arid environments (Alexandrov et al., 2003). Finally, we have little to constrain grain-size distributions further than in Sections 6.1 and 6.2, but using the full range described in those sections (2.2–12 cm) we obtain a range of 75–365 terrestrial years for continuous fluvial deposition.

An alternative hypothesis, that of fluvial transport through a narrow (channel-to-valley ratio $\leqslant$0.09), smooth (roughness coefficient, $r = \sim$0.5 m, see calculation of friction factor in Table 3), bedrock channel carrying large ($\sim$0.5 m diameter) sediment, a scenario that minimizes fluid flux, yields fluid fluxes around $\sim 3 \times 10^4$ m^3 s^{-1}, which is barely compatible with the fluid fluxes calculated

Table 7
Outlet fluid flux comparison. A summary of the slopes and channel widths used to calculate the fluid flow through the inverted channel that continues on from the outlet channel, based on either a sand channel or a gravel channel (the assumptions made for these channels, including the Darcy–Weisbach friction factor and width-to-depth ratios are given in Table 3). The sediment sizes (which affect the Darcy–Weisbach friction factor and thus the flow rate) are given and are derived from martian lander observations (see Table 5).

	Minimum flux	Maximum flux
Variable	*Value*	*Value*
Slope	0.005	0.005
Channel width (m)	280	320
Gravel channel	*Fluid flux (m^3 s^{-1})*	*Fluid flux (m^3 s^{-1})*
2.2 cm	6.6×10^3	9.4×10^3
12 cm	4.9×10^3	7.1×10^3
Sand channel	*Fluid flux (m^3 s^{-1})*	*Fluid flux (m^3 s^{-1})*
.04 mm[a]	7.4×10^3	1.0×10^4
2.0 mm[b]	5.0×10^3	7.0×10^3

[a] The minimum sand diameter, from Herkenhoff et al. (2004).
[b] The maximum particle size for which particles are still defined as being sand (Wentworth, 1922).

for the outlet channel (see Section 6.3). This scenario is less favorable because the sediment concentration is lower than would be expected for floods in semi-arid environments (Alexandrov et al., 2003) and requires a large roughness scale. This scenario gives timescale estimates for the construction of the fluvial fill in Milna on the order of decades.

7. Intermittency of fluvial activity

In Section 6 we explored the total integrated time required to construct the fluvial fill in Milna Crater, assuming continuous flooding conditions. We found that the timescale most compatible with the crater morphology, valley morphologies of the inlet valley, outlet valley, and valleys in the interior of Milna, is hundreds of years. This can now be put into regional and global context by (i) considering the fluvial history of Paraná Valles (e.g. Hynek and Phillips, 2003; Irwin et al., 2007; Barnhart et al., 2009) and (ii) the rates of drainage area erosion as compared to average Noachian erosion rates (see Golombek et al., 2006). Since Milna is located within the catchment of Paraná Valles (see Barnhart et al., 2009), the fluvial histories of both locations are likely to be intimately tied. Taking a cue from the fact that the majority of the shaping of the landscape by fluvial activity on Earth takes place during periodic pulses (Wolman and Miller, 1960) and the fact that the morphology of the nearby Paraná Valles has been found to be incompatible with conditions of constant fluvial activity (Barnhart et al., 2009), we explore the likelihood that periodic, non-constant, fluvial events acted to construct the fluvially derived fill in Milna Crater.

We consider timescales of 10^5–10^6 yr as the total epoch of time over which intermittent fluvial activity occurred, the timing calculated for the formation of Paraná Valles (e.g. Irwin et al., 2007; Barnhart et al., 2009). To check whether timescales of this magnitude are reasonable, the erosion rate (E) can be calculated by dividing the total volume of fluvially derived sediment (V_s, see Table 6) minus the volume of the inlet valley (V_{inlet}) by the surface area of the drainage area sourcing Milna (A; Fig. 6) and the total epoch of erosion (T_e):

$$E = \frac{V_s - V_{inlet}}{AT_e} \quad (14)$$

For the preferred hypothesis the volume of fluvially derived sediment in Milna is 80 km^3, the volume of the inlet valley is 4 km^3, and the drainage area is 3.5×10^4 km^2, so eroding that material over an epoch of 10^5–10^6 yr corresponds to erosion rates of $\sim 10^{-5}$–10^{-6} m/yr (see Table 8). These rates are commensurate with the average Noachian erosion rates of 10^{-5}–10^{-6} m/yr reported in Golombek et al. (2006), although these erosion rates were unlikely to have been constant (cf. Farley et al., 2013). Erosion was also likely higher during periods of fluvial activity and on steeper than average slopes.

Table 8
Calculating activity frequency. Based on the scenarios presented in Table 6 (Minimum, Maximum, Preferred), the fraction of time under which a significant amount of sediment is transported is calculated. The time fraction for sediment transport is calculated by dividing the continuous sediment transport timescales presented in Table 6 by the timescales of regional fluvial activity (either 10^5 or 10^6 years; see Barnhart et al. (2009)). The thickness of eroded material from the drainage area (see Table 6) is divided by either 10^5 yr or 10^6 yr to obtain the long-term average erosion rate of the drainage area, to take into account intermittency of fluvial activity.

	Minimum	Maximum	Preferred
Faster			
Paraná (10^5 yr)	0.02%	4.70%	.08–.37%
Calculated erosion (m/yr)	2×10^{-5}	4×10^{-5}	2×10^{-5}
Slower			
Paraná (10^6 yr)	0.002%	0.47%	.008–.037%
Calculated erosion (m/yr)	2×10^{-6}	4×10^{-6}	2×10^{-6}

Using the preferred timescale for the total integrated time to construct the fluvial fill in Milna, 75–365 yr, and considering that Paraná Valles experienced fluvial reworking over a period of 10^5–10^6 yr, then the majority of sedimentary reworking in Milna took place within the bounds of (i) 8×10^{-5} of the time over 10^6 yr and (ii) 4×10^{-3} of the time over 10^5 yr (see Table 8).

8. Discussion

8.1. Scenarios of intermittency

In this section we explore two scenarios of intermittent fluvial activity compatible with an intermittency factor of 8×10^{-5} to 4×10^{-3} ($\sim$0.008–0.4%) over a period of 10^5–10^6 yr. This intermittency factor is for the timing between significant sediment transport events, not necessarily between water transport events.

Barnhart et al. (2009) suggest that, in order to explain the paucity of crater rim breaches in the Paraná Valles and the southern highlands in general, enough time had to elapse between fluvial inundations to allow for evaporation such that craters did not overflow and form rim incisions. Using their findings from a global hydrologic routing model Matsubara et al. (2011) also find that a single persistent deluge event is incompatible with global-scale morphology. Thus, these authors invoke moderate and episodic flooding events during the Noachian to explain the geomorphology of the southern highlands.

8.1.1. Continuously wet conditions

One possible scenario for the formation of the sedimentary features in Milna is a continuously stable (during 10^5–10^6 yr) climate conducive to fluvial modification. An intermittency frequency of $\sim$0.008–0.4% corresponds to a range in which the fluvial activity responsible for the majority of the work on the landscape recurs between a few days every martian year to about one day every martian decade.

On Earth, bankfull flows in humid to semi-arid environments recur approximately once every 1–2.5 yr. for a few days to a few weeks (several 0.1% to several percent), depending on local climate and catchment size (e.g. Woodyer, 1968). However, in arid environments channel morphology can be set by hours-long storms on decadal timescales (a few 0.01%) (Woodyer, 1968; Baker, 1977). The intermittency we calculate for Milna is compatible with semi-arid to arid environments, or a climate where nearly all of the sediment transport takes place during short-duration floods with recurrence intervals of years to decades.

Such a long-term climate as we are exploring here would probably require precipitation (e.g. discussions in Lamb et al., 2006; Andrews-Hanna et al., 2007; Di Achille et al., 2007; Irwin et al., 2007). We can calculate the depth of precipitation (P) required to generate the fluid flux (Q) required in the preferred scenario laid out in Table 6, given the percent of precipitation lost to evaporation during runoff to Milna (L) in the drainage area (A). After choosing a timescale for the precipitation event (t_p), we have:

$$P = \frac{Qt_p}{A(1-L)} \quad (15)$$

Typical terrestrial loss fractions (L) range from $\sim$10% to 60% (Gibson and Edwards, 2002). Under our preferred conditions we find that 0.5–5 cm of rainfall in an event lasting one day would be required to generate appropriate fluid fluxes (see Table 9), although flooding could also be caused by other processes, e.g. melt runoff.

We can subject this scenario to one last calculation. Matsubara et al. (2011) use a global hydrologic routing model to constrain the ratio of precipitation to evaporation (ε) using what they call an "X-ratio," where X is the ratio between net evaporation off a lake

Table 9
Precipitation rates required for preferred scenario (Table 6). The thickness of precipitation required over the entire drainage area (A) during one day (t_p) to obtain the fluid fluxes through the inlet channel (according to the preferred scenario in Table 6), given a particular loss rate back to the atmosphere by evaporation off of the drainage area (L).

Precipitation (cm)	A (km^2)	L	Q (m^3 s^{-1})	t_p
0.5	3.5×10^4	0.1	2×10^3	day
1	3.5×10^4	0.6	2×10^3	day
2	3.5×10^4	0.1	8×10^3	day
5	3.5×10^4	0.6	8×10^3	day

and runoff depth in its contributing drainage basin. By accounting for the ratio of the drainage area to the area of the paleolake (A_L; in Milna A_L is about 1.7% the drainage area), a rearrangement of their equation gives the rate at which evaporation should be expected from the paleolake, using X and the period of time between bankfull storms (f_p):

$$\varepsilon = \frac{(1 + X(1 - L))P}{(A_L/A)}\left(\frac{t_p}{f_p}\right) \tag{16}$$

We assume that precipitation during the rest of the time does not, in total, exceed the total precipitation from storm events that set the morphology of the landscape and use the range of X-ratios reported for Mars by Matsubara et al. (2011) (X between 3.1 and 7.7, a range over which lakes would maintain a standing body of water), which are based on a hydrologic balance within basins that includes runoff, throughflow, evaporation, infiltration, and intrabasin groundwater flow, but neglect the minor contribution of inter-basin groundwater transfer (Matsubara et al., 2011). This calculation gives evaporation rates that range from 0.16 to 17 meters per terrestrial year (see Table 10), although these evaporation rates do not include transpiration by plants, which plays an important part in terrestrial evaporation rates. Typical terrestrial evaporative loss rates of lakes across a wide range of climates are on the order of meters per year (e.g. Farnsworth and Thompson, 1983; Morton, 1983). Thus the range of water fluxes we obtain for the construction of the fluvial fill at Milna are compatible with the evaporation and precipitation rates modeled by Matsubara et al. (2011), assuming that evaporation rates on Mars during the time that Milna formed are comparable to the range of evaporation rates we see on Earth today.

8.1.2. Periodic flooding from giant impacts

An alternative scenario that also fits the regional constraints and the morphology we see at Milna are moderate floods that occur infrequently and last for longer periods of time, without the need for fluvial activity in between. The work of Barnhart et al. (2009) and Matsubara et al. (2011) indicate that deluge conditions should take place for less than about one decade in order to be consistent with the morphology of the martian southern highlands.

Although the regional constraints and morphology of Milna allow this scenario, further consideration can be given to the mechanism that would cause such deluges, and we can consider the effect of environmental conditions created by giant impacts. Giant impacts would create a climate conducive to precipitation for between (i) tens of days, releasing a total of ~40 cm of water, assuming a ~30 km impactor and (ii) several years, releasing a total of ~10 m total of water per unit area, assuming a ~100 km impactor (Segura et al., 2008). Segura et al. (2008) suggest that this water comes from vaporized water originating in the impactor and the impact target site and from global evaporation of water and ice while vaporized rock created by the impact is in the atmosphere.

The total volume of fluid required to carry the sediment necessary to construct the sedimentary fill in Milna under conditions of continuous fluid delivery can be estimated by calculating the amount of fluid involved in the minimum timescale scenarios (Table 6). This calculation indicates that $\sim 4 \times 10^{12}$ m^3 of water is required (the flux of water times the total duration of the flux). This is a minimum estimate of the water required to create the fluvial fill in Milna since regimes of flow with lower flux require even more water because the sediment concentration is lower (e.g. ~an order of magnitude more water, 2×10^{13} m^3, is required for our preferred hypothesis; see Table 6). If we assume that a 100 km bolide triggered a deluge event under a 1-bar CO_2 atmosphere (using the values that produce maximum rainfall of those given in Segura et al., 2008), there would be ~10 m of water per unit area over the entire drainage area (3.5×10^4 km^2), or $\sim 3 \times 10^{11}$ m^3. This is one order of magnitude lower than the minimum water volume required to construct the sedimentary fill in Milna, so approximately ten 100 km bolide impacts (corresponding to ten deluge events) would be required for the construction of the fill in Milna. This is an unlikely scenario since most of the giant impact basins were formed prior to ~3.8 Gyr (e.g. Roberts et al., 2009), which would put this mechanism at odds with the ages of martian valley networks (Fassett and Head, 2008a).

Since smaller craters impact more frequently, we could also estimate the volume of mobile water created by 'small' impacts. A 30 km impactor colliding with Mars under a 150-mbar atmosphere would produce ~36 cm of rain (Segura et al., 2008). This translates into $\sim 1 \times 10^{10}$ m^3 of water in the drainage area sourcing Milna, about two orders of magnitude less than the minimum we calculate is required to transport the sedimentary fill into Milna,

Table 10
Evaporation rate based on X-ratio. Evaporation rates are calculated using a modification of the equation to derive the X-ratio, a quantity relating the rates of precipitation and evaporation, from Matsubara et al. (2011). A higher X-ratio indicates a relatively higher evaporation rate as compared to the precipitation rate. The calculations are placed in two categories, which consider the evaporation implied by the precipitation rates given in Table 9 and the X-ratio found by Matsubara et al. (2011): Minimum (lower precipitation and lower X-ratio) and Maximum (higher precipitation and higher X-ratio). Total precipitation between storm events (twice the total precipitation thickness during a single storm event, as given in Table 9; discussed in Section 8.1.1) is given. The loss rate back to the atmosphere by evaporation off of the drainage area (L) is tied to the calculations of minimum and maximum precipitation shown in Table 9, and is kept consistently as it is used in Eqs. (15) and (16). The storm frequency is given in martian years and is required to determine the rate of evaporation relative to the rate of total precipitation. The X-ratios are the minimum and maximum reported by Matsubara et al. (2011).

Total precipitation per storm event (P, cm)	L	f_p (martian years between storm event)	X	ε (m yr^{-1})[a]
Minimum evaporation				
1	0.1	1	3.1	1.6
1	0.1	2.5	3.1	0.64
1	0.1	10	3.1	0.16
Maximum evaporation				
10	0.6	1	7.7	17
10	0.6	2.5	7.7	6.8
10	0.6	10	7.7	1.7

Years are terrestrial years.
[a] Evaporation rate is converted to terrestrial years to facilitate comparison with terrestrial rates.

implying that ∼100 of these impacts would be required to generate enough water to create the fill in Milna. Segura et al. (2008) calculate that a bolide ⩾10 km would impact onto Mars every 1–10 Myr between 3 and 4 Gyr ago. Using these values translates to timescales of 100 My to 1 Gyr for the formation of the sedimentary deposit in Milna, which is 2–3 orders magnitude longer than the estimates for the formation of nearby Paraná Valles (Barnhart et al., 2009). If the preferred hypothesis (Section 6.4) is used, the amount of water required to transport sediment diverges by even another order of magnitude from the estimated amount of water delivered to Milna by impactors.

Thus, it seems improbable that impacts alone would mobilize enough water to create the sedimentary features observed in Milna. If discrete, periodic floods were responsible for the deposition of the sedimentary fill in Milna, then it appears that a mechanism other than (or in addition to) impact generated climate change needs to be invoked.

8.2. Additional regional context

The other large (>10 km diameter) craters within several hundred kilometers of Milna do not show the same extent of fluvial modification as Milna (see Fig. 1). However, this is unsurprising because the drainage area leading to Milna is much larger than the drainage areas of these other craters (Fig. 6) and therefore does not imply that fluvial processes in this area were locally constrained to affect only Milna. Indeed, the Margaritifer Sinus Quadrangle (in which Milna is located) has been modified extensively by fluvial activity (e.g. Craddock et al., 1997; Grant, 2000; Grant and Parker, 2002; Irwin et al., 2005a) and there are several sinuous valleys within the area captured in Fig. 1, as well as other open basin paleolakes within the Margaritifer Sinus Quadrant (e.g. Howard et al., 2005; Fassett and Head, 2008a, 2008b).

Additionally, there are numerous filled-in 'ghost craters' within a few hundred square kilometers of Milna (Fig. 1 shows locations

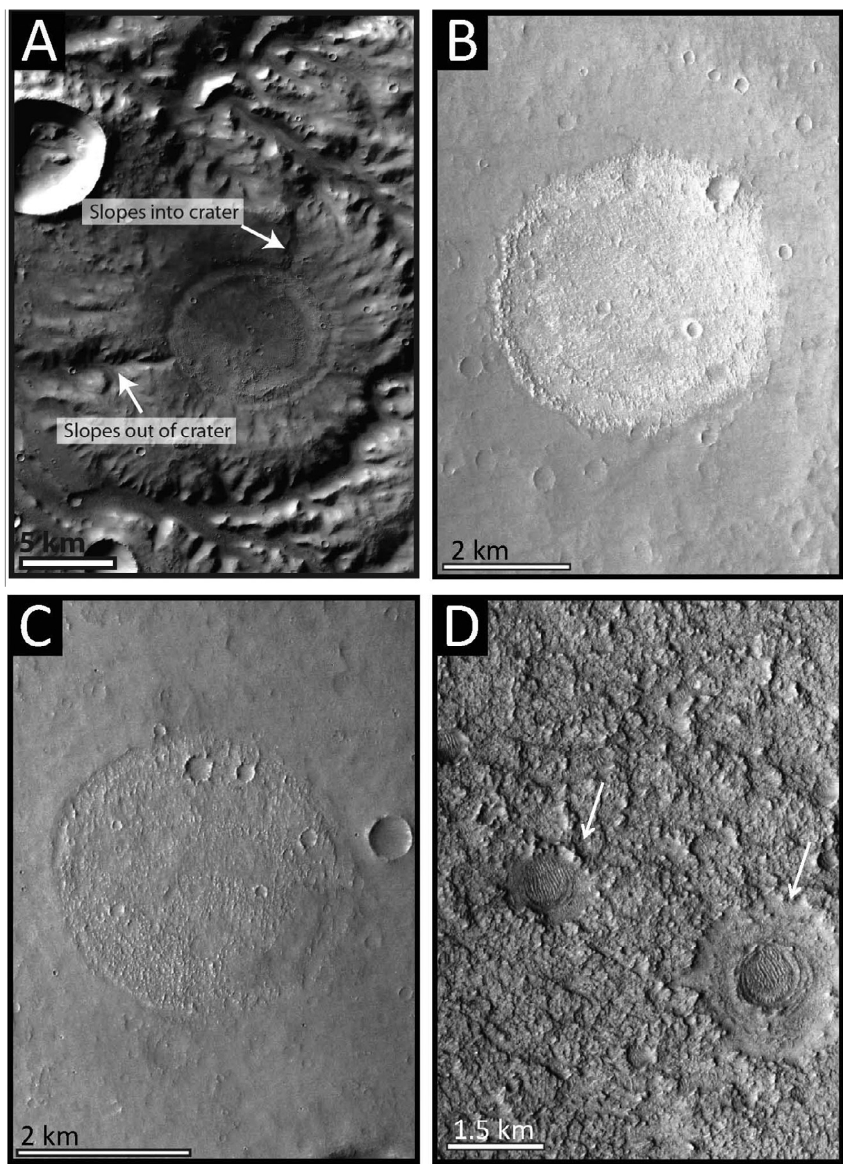

Fig. 7. (A) 'Ghost crater' in Paraná Valles with a valley sloping into it and a valley sloping out of it. Note that the texture inside the crater is hummocky and different than the surrounding texture. This crater also appears in Fig. 15 of Howard et al. (2005). (B and C) 'Ghost craters' in the drainage area leading to Milna. 'Ghost craters,' as they were identified in Fig. 1, are roughly circular features with a hummocky texture and little to no vertical relief relative to the surrounding terrain. (D) Hummocky texture in the prominent impact crater at the bottom center of the drainage area sourcing Milna. Note that the craters that impacted into the hummocky surface have a dune texture that is clearly different than the hummocky texture. *Images are (A) CTX (P21_009049_1580, (B–D) CTX (P01_001586_1563).*

of ghost craters identified in this paper; Fig. 7 illustrates how ghost craters were identified), including in the drainage area corresponding to Milna (Figs. 1 and 6). 'Ghost' craters are shallow, flat-rimmed craters that have been interpreted to be extensively filled-in by a variety of geologic processes (e.g. McGill and Wise, 1972; Arvidson, 1974; Craddock and Maxwell, 1993; Mangold, 2003; Tanaka et al., 2003; Howard et al., 2005). We identify ghost craters in the Paraná Valles region as roughly circular features with a hummocky texture and little to no topographic relief. Within the Paraná Valles region some of these ghost craters have an inlet valley and an outlet valley, like open basin paleolakes, and the texture of the fill is consistent with fluvial deposition (Fig. 7, cf. Irwin et al., 2007). Unlike other accepted open basin paleolakes, however, the basins of 'ghost' craters have been entirely filled, which can be expected because infilling is a common limit on the lifetime of lakes on Earth (Cohen, 2003) and modeling of regional fluvial activity on Mars predicts these 'ghost' craters as the result of widespread sediment redistribution by water (see Craddock and Howard, 2002). These craters are further indicators of widespread fluvial activity in the region, and a further study of their distribution may yield useful information about the fluvial history of at least the Paraná Valles region.

8.3. Discussion of timescales

We calculate geologically short timescales both for flooding Milna with fluid and for constructing the sedimentary fill in Milna. While calculating the flooding time does give minimum estimates for the timescale of fluvial activity required to construct the inlet and outlet breaches that are indicative of an open basin paleolake (Fassett and Head, 2008b), the flooding timescales we calculate are always at least two orders of magnitude smaller than the sedimentary fill construction timescales. Also, continuous flooding conditions are unlikely to be responsible for the formation for all martian paleolakes and are inconsistent with many of the hydrological signatures on Mars, such as interior channels (e.g. Irwin et al., 2005a; Penido et al., 2013), physical laws governing erosion in valleys by fluids (e.g. Wilson et al., 2004), multilobed and incised fans (e.g. this paper), layered fan deposits (e.g. Fassett et al., 2007) and the degree of regional erosion and drainage integration (e.g. discussions in Barnhart et al., 2009).

Our data favor a short (hundreds of years) integrated continuous timing of fluvial activity in order to form the lake and sedimentary deposit in Milna. In order to reconcile this timescale with the regional geomorphology and average Noachian erosion rates, it appears that fluvial activity capable of setting the geomorphology of the landscape was episodic (Section 7). Intermittency is also consistent with the morphology of the sedimentary deposit in Milna, whose fan deposits at different elevations and valleys incising the depositional fans may indicate episodic deposition (Section 3.3). Additionally, the difference in morphology between (i) the initial, underlying sedimentary deposit that forms the bulk of the volume of the deposit and lacks discrete, distinguishable features and (ii) the five discrete overlying fans (Fans A–E, Section 3.3), may indicate a change in depositional regimes culminating with Fans A–E recording the last several pulses of deposition. Following the discussion in Section 8.1, our preferred hypothesis is that the sedimentary fill in Milna was delivered by intermittent, possibly seasonally recurring bankfull storms sourced by precipitation events delivering water at cm/day rates recurring approximately every martian year to martian decade for 10^5–10^6 yr.

Several authors have made estimates about the timescale of active martian hydrology, ranging from 'short,' persistent localized events that take days to hypotheses based on regional trends that argue for 'long' periods of periodic active hydrology on the scale of 10^8 years (Table 1). Our results are consistent both with fluvial processes occurring over short periods of time and long periods of time (up to $\sim 10^6$ yr), and our calculation of intermittency rates can be used to help quantitatively reconcile the wide range of measurements of the timescales of fluvial activities on Mars (Table 1). However, it is important to keep in mind that even the comparatively 'long' estimates of millions of years for active hydrologic activity on Mars are still just a small blip ($\sim$0.1%) in the whole geologic history of Mars (e.g. Kleinhans, 2005) and that the martian climate may have varied from place to place, as it does on Earth.

9. Conclusion

Milna Crater, centered at (23.4S, 12.3W), exhibits a complex set of sedimentary fan deposits incised by sinuous valleys. These fans, in conjunction with inlet and outlet channels and the dimensions of the crater, are evidence that Milna once housed a lake with a volume of at least 50 km^3. The complex sedimentary deposit indicates that there were several stages of fluvial activity in Milna: deposition of an initial fan complex, which was then partially dissected by valleys, leading to additional fan deposits that were emplaced as water levels in the paleolake rose and fell.

We calculate that 15–4700 yr of total integrated fluvial activity is required to construct the fluvial sedimentary fill in Milna (taking into account potential other sources of fill). We find that sediment construction timescales are more than two orders of magnitude greater than the time required to simply flood the crater cavity with fluid. By placing the fluvial activity at Milna in a regional and global context, comparing it to the quantitative calculations of activity in Paraná Valles and Noachian erosion rates, indicates that the fluvial activity in Milna likely took place over 10^5–10^6 yr. This, coupled with the discrete fan deposits inside Milna, strongly suggests that periods of fluvial activity were intermittent. Our preferred hypothesis is that fluvial activity took place intermittently, possibly with seasonal or decadal storms that operated to produce significant fluvial deposition $\sim$0.01–0.1% of the time over the 10^5–10^6 yr the lifetime of the system.

Our findings for the first time provide a quantitative intermittency factor that can help bridge the gap between the calculations of short and long timescales of fluvial activity on Mars reported in the literature. The methods we apply here can be used in other open basin paleolakes to further aid our understanding of the timescales of fluvial activity on Mars.

Acknowledgments

Elucidating discussions with Laura Kerber and assistance from Jay Dickson facilitated and improved this investigation. Input from Tim Goudge and two anonymous reviewers helped to improve this paper, and is greatly appreciated. PBB is thankful for funding from the California Institute of Technology Summer Undergraduate Research Fellowship program and from the Brown University Geosciences Department. We gratefully acknowledge the financial assistance of the NASA Mars Data Analysis Program Grant NNX11AI81G and participation in the Mars Express High Resolution Stereo Camera (HRSC) Team through JPL1237163, both to JWH. MPL acknowledges support from NASA Grant 12PGG120107.

References

Alexandrov, Y., Laronne, J.B., Reid, I., 2003. Suspended sediment concentration and its variation with water discharge in a dryland ephemeral channel, northern Negev, Israel. J. Arid Environ. 53, 73–84. http://dx.doi.org/10.1006/jare.2002.1020.

Andrews-Hanna, J.C., Phillips, R.J., Zuber, M.T., 2007. Meridiani Planum and the global hydrology of Mars. Nature 446, 163–166. http://dx.doi.org/10.1038/nature05594.

Armitage, J.J., Warner, N.H., Goddard, K., Gupta, S., 2011. Timescales of alluvial fan development by precipitation on Mars. Geophys. Res. Lett. 38, L17203. http://dx.doi.org/10.1029/2011GL048907.

Arvidson, R.E., 1974. Morphologic classification of martian craters and some implications. Icarus 22, 264–271. http://dx.doi.org/10.1016/0019-1035(74)90176-6.

Baker, V.R., 1977. Stream-channel response to floods, with examples from central Texas. Geol. Soc. Am. Bull. 88, 1057–1071. http://dx.doi.org/10.1130/0016-7606(1977) 88.

Baker, V.R., Milton, D.J., 1974. Erosion by catastrophic floods on Mars and Earth. Icarus 23, 27–41.

Barnhart, C.J., Howard, A.D., Moore, J.M., 2009. Long-term precipitation and late-stage valley network formation: Landform simulations of Parana Basin, Mars. J. Geophys. Res. 114, E01003. http://dx.doi.org/10.1029/2008JE003122.

Bathurst, J.C., 1993. Flow resistance through the channel network. In: Beven, K., Kirk, M.J. (Eds.), Channel Network Hydrology. John Wiley, New York, pp. 69–98.

Bhattacharya, J.P., Payenberg, T.H.D., Lang, S.C., Bourke, M., 2005. Dynamic river channels suggest a long-lived Noachian crater lake on Mars. Geophys. Res. Lett. 32, L10201. http://dx.doi.org/10.1029/2005GL022747.

Buhler, P.B., Fassett, C.I., Head, J.W., Lamb, M.P., 2011. Paleolakes in Erythraea Fossa, Mars: Implications for an ancient active hydrological cycle. Icarus 2011. http://dx.doi.org/10.1016/j.icarus.2011.03.004.

Burr, D.M., Enga, M., Williams, R.M.E., Zimbelman, J.R., Howard, A.D., Brennand, T.A., 2009. Pervasive aqueous paleoflow features in the Aeolis/Zephyria Plana region, Mars. Icarus 200, 52–76. http://dx.doi.org/10.1016/j.icarus.2008.10.014.

Cabrol, N.A., Grin, E.A., 1999. Distribution, classification, and ages of martian impact crater lakes. Icarus 142, 160–172. http://dx.doi.org/10.1006/icar.1999.6191.

Carr, M.H., 2012. The fluvial history of Mars. Philos. Trans. R. Soc. A 370, 2193–2215. http://dx.doi.org/10.1098/rsta.2011.0500.

Carr, M.H., Clow, G.D., 1981. Martian channels and valleys: Their characteristics, distribution, and age. Icarus 48, 91–117. http://dx.doi.org/10.1016/0019-1035(81)90156-1.

Christensen, P.R. et al., 2003. Morphology and composition of the surface of Mars: Mars Odyssey THEMIS results. Science 300, 2056–2061. http://dx.doi.org/10.1126/science.1080885.

Cohen, A., 2003. Paleolimnology: The History and Evolution of Lake Systems. Oxford University Press, pp. 21–55.

Craddock, R.A., Howard, A.D., 2002. The case for rainfall on a warm, wet early Mars. J. Geophys. Res. 107, 5111. http://dx.doi.org/10.1029/2001JE001505.

Craddock, R.A., Maxwell, T.A., 1993. Geomorphic evolution of the martian highlands through ancient fluvial processes. J. Geophys. Res. 98, 3453–3468. http://dx.doi.org/10.1029/92JE02508.

Craddock, R.A., Maxwell, T.A., Howard, A.D., 1997. Crater morphometry and modification in the Sinus Sabaeus and Margaritifer Sinus regions of Mars. J. Geophys. Res. 102, 13321–13340. http://dx.doi.org/10.1029/97JE01084.

Daly, R.A., Manger, G.E., Clark, S.P., 1966. Section 4: Density of rocks. Geol. Soc. Am. Memoirs 97, 19–26. http://dx.doi.org/10.1130/MEM97-p19.

De Hon, R.A., 1992. Martian lake basins and lacustrine plains. Earth Moon Planets 56, 95–122. http://dx.doi.org/10.1007/BF00056352.

De Villiers, G., Kleinhans, M.G., Postma, G., 2013. Experimental delta formation in crater lakes and implications for interpretation of martian deltas. J. Geophys. Res.: Planets 118, 651–670. http://dx.doi.org/10.1002/jgre.20069.

Di Achille, G., Ori, G.G., Reiss, D., 2007. Evidence for Late Hesperian lacustrine activity in Shalbatana Vallis, Mars. J. Geophys. Res. 112, E07007. http://dx.doi.org/10.1029/2006JE002858.

Di Achille, G., Hynek, B.M., Searls, M.L., 2009. Positive identification of lake strandlines in Shalbatana Vallis, Mars. Geophys. Res. Lett. 36, L14201. http://dx.doi.org/10.1029/2009GL038854.

DiBiase, R.A., Limaye, A.B., Scheingross, J.S., Fischer, W.W., Lamb, M.P., 2013. Deltaic deposits at Aeolis Dorsa: Sedimentary evidence for a standing body of water on the northern plains of Mars. J. Geophys. Res.: Planets 118, 1–18. http://dx.doi.org/10.1002/jgre.20100.

Duck, R.W., McManus, J., 1994. A long-term estimate of bedload and suspended sediment yield derived from reservoir deposits. J. Hydrol. 159, 365–373. http://dx.doi.org/10.1016/0022-1694(94)90267-4.

Ehlmann, B.L. et al., 2008. Clay minerals in delta deposits and organic preservation potential on Mars. Nat. Geosci. 1, 355–358. http://dx.doi.org/10.1038/ngeo207.

Farley, K.A. et al., 2013. In situ radiometric and exposure age dating of the martian surface. Science 1247166. http://dx.doi.org/10.1126/science.1247166.

Farnsworth, R.K., Thompson, E.S., 1983. Mean Monthly, Seasonal, and Annual Pan Evaporation for the United States. US Department of Commerce, National Oceanic and Atmospheric Administration, National Weather Service.

Fassett, C.I., Head, J.W., 2005. Fluvial sedimentary deposits on Mars: Ancient deltas in a crater lake in the Nili Fossae region. Geophys. Res. Lett. 32, L14201. http://dx.doi.org/10.1029/2005GL023456.

Fassett, C.I., Head, J.W., 2008a. The timing of martian valley network activity: Constraints from buffered crater counting. Icarus 195, 61–89. http://dx.doi.org/10.1016/j.icarus.2007.12.009.

Fassett, C.I., Head, J.W., 2008b. Valley network-fed, open-basin lakes on Mars: Distribution and implications for Noachian surface and subsurface hydrology. Icarus 198, 37–56. http://dx.doi.org/10.1016/j.icarus.2008.06.016.

Fassett, C.I., Ehlmann, B.L., Head, J.W., Mustard, J.F., Schon, S.C., Murchie, S.L., 2007. Sedimentary fan deposits in Jezero Crater Lake, in the Nili Fossae Region, Mars: Meter-scale layering and phyllosilicate-bearing sediments. American Geophysical Union (Fall) Meeting 2007, #P13D-1562.

Ferguson, R.I., Church, M., 2004. A simple universal equation for grain settling velocity. J. Sediment. Res. 74, 933–937. http://dx.doi.org/10.1306/051204740933.

Fernandez Luque, R., van Beek, R., 1976. Erosion and transport of bed-load sediment. J. Hydraul. Res. 14, 127–144. http://dx.doi.org/10.1080/00221687609499677.

Finnegan, N.J., Roe, G., Montgomery, D.R., Hallet, B., 2005. Controls on the channel width of rivers: Implications for modeling fluvial incision of bedrock. Geology 33, 229–232. http://dx.doi.org/10.1130/G21171.1.

Forsberg-Taylor, N.K., Howard, A.D., Craddock, R.A., 2004. Crater degradation in the martian highlands: Morphometric analysis of the Sinus Sabaeus region and simulation modeling suggest fluvial processes. J. Geophys. Res. 109, E05002. http://dx.doi.org/10.1029/2004JE002242.

Gaidos, E., Marion, G., 2003. Geological and geochemical legacy of a cold early Mars. J. Geophys. Res. 108, 5055. http://dx.doi.org/10.1029/2002JE002000.

Garvin, J.B., Sakimoto, S.E.H., Frawley, J.J., Schnetzler, C., 2000. North polar region craterforms on Mars: Geometric characteristics from the Mars Orbiter Laser Altimeter. Icarus 144, 329–352. http://dx.doi.org/10.1006/icar.1999.6298.

Garvin, J.B., Sakimoto, S.E.H., Frawley, J.J., Schnetzler, C., 2002. Global geometric properties of martian impact craters. Lunar Planet. Sci. XXXIII, 1255.

Garvin, J.B., Sakimoto, S.E.H., Frawley, J.J., 2003. Craters on Mars: Global geometric properties from gridded MOLA topography. In: Sixth International Conference on Mars, 3277.

Gibson, J.J., Edwards, T.W.D., 2002. Regional water balance trends and evaporation–transpiration partitioning from a stable isotope survey of lakes in northern Canada. Glob. Biogeochem. Cycl. 16. http://dx.doi.org/10.1029/2001GB001839.

Goldspiel, J.M., Squyres, S.W., 1991. Ancient aqueous sedimentation on Mars. Icarus 89, 392–410. http://dx.doi.org/10.1016/0019-1035(91)90186-W.

Golombek, M.P. et al., 2003. Rock size–frequency distributions on Mars and implications for Mars Exploration Rover landing safety and operations. J. Geophys. Res. 108, 8086. http://dx.doi.org/10.1029/2002JE002035.

Golombek, M.oP. et al., 2006. Erosion rates at the Mars Exploration Rover landing sites and long-term climate change on Mars. J. Geophys. Res. 111, E12S10. http://dx.doi.org/10.1029/2006JE002754.

Grant, J.A., 2000. Valley formation in Margaritifer Sinus, Mars, by precipitation-recharged ground-water sapping. Geology 28, 223–226. http://dx.doi.org/10.1130/0091-7613(2000) 28.

Grant, J.A., Parker, T.J., 2002. Drainage evolution in the Margaritifer Sinus region, Mars. J. Geophys. Res. 107, 5066. http://dx.doi.org/10.1029/2001JE001678.

Grin, E.A., Cabrol, N.A., 1997. Limnologic analysis of Gusev Crater paleolake, Mars. Icarus 130, 461–474. http://dx.doi.org/10.1006/icar.1997.5817.

Grotzinger, J.P., and Athena Science Team, 2004. Stratification, sediment transport, and the early wet surface of Meridiani Planum. American Geophysical Union (Fall). Eos (Suppl.) 85(47). Abstract P24A-01.

Herkenhoff, K.E. et al., 2004. Textures of the soils and rocks at Gusev Crater from Spirit's Microscopic Imager. Science 305, 824–826. http://dx.doi.org/10.1126/science.1100015.

Hoke, M.R.T., Hynek, B.M., Tucker, G.E., 2011. Formation timescales of large martian valley networks. Earth Planet. Sci. Lett. 312, 1–12. http://dx.doi.org/10.1016/j.epsl.2011.09.053.

Howard, A.D., Moore, J.M., Irwin, R.P., 2005. An intense terminal epoch of widespread fluvial activity on early Mars: 1. Valley network incision and associated deposits. J. Geophys. Res. 110, E12S14. http://dx.doi.org/10.1029/2005JE002459.

Hynek, B.M., Phillips, R.J., 2003. New data reveal mature, integrated drainage systems on Mars indicative of past precipitation. Geology 31, 757–760. http://dx.doi.org/10.1130/G19607.1.

Irwin, R.P., Craddock, R.A., Howard, A.D., 2005a. Interior channels in martian valley networks: Discharge and runoff production. Geology 33, 489–492. http://dx.doi.org/10.1130/G21333.1.

Irwin, R.P., Howard, A.D., Craddock, R.A., Moore, J.M., 2005b. An intense terminal epoch of widespread fluvial activity on early Mars: 2. Increased runoff and paleolake development. J. Geophys. Res.: Planets 110, E12. http://dx.doi.org/10.1029/2005JE002460.

Irwin, R.P., Maxwell, T.A., Howard, A.D., 2007. Water budgets on early Mars: Empirical constraints from paleolake basin and watershed areas. LPI Contribution No. 1353, p. 3400.

Jerolmack, D.J., Mohrig, D., Zuber, M.T., Byrne, S., 2004. A minimum time for the formation of Holden Northeast fan, Mars. Geophys. Res. Lett. 31, L21701. http://dx.doi.org/10.1029/2004GL021326.

Kite, E.S., Lucas, A., Fassett, C.I., 2013. Pacing early Mars river activity: Embedded craters in the Aeolis Dorsa region imply river activity spanned $\gtrsim$(1–20) Myr. Icarus 225, 850–855. http://dx.doi.org/10.1016/j.icarus.2013.03.029.

Kleinhans, M.G., 2005. Flow discharge and sediment transport models for estimating a minimum timescale of hydrological activity and channel and delta formation on Mars. J. Geophys. Res. 110, E12003. http://dx.doi.org/10.1029/2005JE002521.

Kleinhans, M.G., van de Kasteele, H.E., Hauber, E., 2010. Palaeoflow reconstruction from fan delta morphology on Mars. Earth Planet. Sci. Lett. 294, 378–392. http://dx.doi.org/10.1016/j.epsl.2009.11.025.

Komar, P.D., 1979. Comparisons of the hydraulics of water flows in martian outflow channels with flow of similar scale on Earth. Icarus 37, 156–181. http://dx.doi.org/10.1016/0019-1035(79)90123-4.

Komatsu, G., Baker, V.R., 1997. Paleohydrology and flood geomorphology of Ares Vallis. J. Geophys. Res.: Planets 102, 4151–4160. http://dx.doi.org/10.1029/96JE02564.

Kraal, E.R., van Dijk, M., Postma, G., Kleinhans, M.G., 2008. Martian stepped-delta formation by rapid water release. Nature 451, 973–976. http://dx.doi.org/10.1038/nature06615.

Lamb, M.P., Howard, A.D., Johnson, J., Whipple, K.X., Dietrich, W.E., Perron, J.T., 2006. Can springs cut canyons into rock? J. Geophys. Res. 111, E7. http://dx.doi.org/10.1029/2005JE002663.

Malin, M.C., Edgett, K.S., 2003. Evidence for persistent flow and aqueous sedimentation on early Mars. Science 302, 1931–1934. http://dx.doi.org/10.1126/science.1090544.

Malin, M.C. et al., 2007. Context Camera investigation on board the Mars Reconnaissance Orbiter. J. Geophys. Res. 112, E05S04. http://dx.doi.org/10.1029/2006JE002808.

Mangold, N., 2003. Geomorphic analysis of lobate debris aprons on Mars at Mars Orbiter Camera scale: Evidence for ice sublimation initiated by fractures. J. Geophys. Res. 108, 8021. http://dx.doi.org/10.1029/2002JE001885.

Mangold, N., Ansan, V., 2006. Detailed study of an hydrological system of valleys, a delta and lakes in the Southwest Thaumasia region, Mars. Icarus 180, 75–87. http://dx.doi.org/10.1016/j.icarus.2005.08.017.

Mangold, N., Kite, E.S., Kleinhans, M.G., Newsom, H., Ansan, V., Hauber, E., Kraal, E., Quantin, C., Tanaka, K., 2012. The origin and timing of fluvial activity at Eberswalde crater, Mars. Icarus 220, 530–551. http://dx.doi.org/10.1016/j.icarus.2012.05.026.

Matsubara, Y., Howard, A.D., 2009. A spatially explicit model of runoff, evaporation, and lake extent: Application to modern and late Pleistocene lakes in the Great Basin region, western United States. Water Resour. Res. 45, W06425. http://dx.doi.org/10.1029/2007WR005953.

Matsubara, Y., Howard, A.D., Drummond, S.A., 2011. Hydrology of early Mars: Lake basins. J. Geophys. Res. 116, E04001. http://dx.doi.org/10.1029/2010JE003739.

Mavko, G., Mukerji, T., Dvorkin, J., 2009. The Rock Physics Handbook: Tools for Seismic Analysis of Porous Media. Cambridge University Press, p. 450.

McEwen, A.S. et al., 2007. Mars Reconnaissance Orbiter's High Resolution Imaging Science Experiment (HiRISE). J. Geophys. Res. 112, E05S02. http://dx.doi.org/10.1029/2005JE002605.

McGill, G.E., Wise, D.U., 1972. Regional variations in degradation and density of martian craters. J. Geophys. Res. 77, 2433–2441. http://dx.doi.org/10.1029/JB077i014p02433.

Metz, J.M. et al., 2009. Sublacustrine depositional fans in southwest Melas Chasma. J. Geophys. Res. 114, E10002. http://dx.doi.org/10.1029/2009JE003365.

Moore, J.M., Howard, A.D., Dietrich, W.E., Schenk, P.M., 2003. Martian layered fluvial deposits: Implications for Noachian climate scenarios. Geophys. Res. Lett. 30, 2292. http://dx.doi.org/10.1029/2003GL019002.

Moratto, Z.M., Broxton, M.J., Beyer, R.A., Lundy, M., Husmann, K., 2010. Ames Stereo Pipeline, NASA's open source automated stereogrammetry software. Lunar Planet. Sci. 41. Abstract 2364.

Morgan, A.M., Howard, A.D., Hobley, D.E.J., Moore, J.M., Dietrich, W.E., Williams, R.M.E., Burr, D.M., Grant, J.A., Wilson, S.A., Matsubara, Y., 2014. Sedimentology and climatic environment of alluvial fans in the martian Saheki crater and a comparison with terrestrial fans in the Atacama Desert. Icarus 229, 131–156. http://dx.doi.org/10.1016/j.icarus.2013.11.007.

Morton, F.I., 1983. Operational estimates of lake evaporation. J. Hydrol. 66, 77–100. http://dx.doi.org/10.1016/0022-1694(83)90178-6.

Neukum, G. et al., 2004. Recent and episodic volcanic and glacial activity on Mars revealed by the High Resolution Stereo Camera. Nature 432, 971–979. http://dx.doi.org/10.1038/nature03231.

Penido, J.C., Fassett, C.I., Som, S.M., 2013. Scaling relationships and concavity of small valley networks on Mars. Planet. Space Sci. 75, 105–116. http://dx.doi.org/10.1016/j.pss.2012.09.009.

Pieri, D.C., 1980. Martian valleys: Morphology, distribution, age, and origin. Science 210, 895–897.

Pratt-Sitaula, B., Garde, M., Burbank, D.W., Oskin, M., Heimsath, A., Gabet, E., 2007. Bedload-to-suspended load ratio and rapid bedrock incision from Himalayan landslide-dam lake record. Quatern. Res. 68, 111–120. http://dx.doi.org/10.1016/j.yqres.2007.03.005.

Roberts, H.H., 1997. Dynamic changes of the Holocene Mississippi River delta plain: The delta cycle. J. Coastal Res. 13 (3), 605–627, ISSN 0749-0208.

Roberts, J.H., Lillis, R.J., Manga, M., 2009. Giant impacts on early Mars and the cessation of the martian dynamo. J. Geophys. Res. 114, E04009. http://dx.doi.org/10.1029/2008JE003287.

Schon, S.C., Head, J.W., Fassett, C.I., 2012. An overfilled lacustrine system and progradational delta in Jezero Crater, Mars: Implications for Noachian climate. Planet. Space Sci. 67, 28–45. http://dx.doi.org/10.1016/j.pss.2012.02.003.

Schumm, S.A., Khan, H.R., 1972. Experimental study of channel patterns. Geol. Soc. Am. Bull. 83, 1755–1770. http://dx.doi.org/10.1130/0016-7606(1972)83.

Segura, T.L., Toon, O.B., Colaprete, A., 2008. Modeling the environmental effects of moderate-sized impacts on Mars. J. Geophys. Res. 113, E11007. http://dx.doi.org/10.1029/2008JE003147.

Smith, D.E. et al., 2001. Mars Orbiter Laser Altimeter: Experiment summary after the first year of global mapping of Mars. J. Geophys. Res. 106, 23689–23722. http://dx.doi.org/10.1029/2000JE001364.

Tanaka, K.L., Skinner Jr., J.A., Hare, T.M., Joyal, T., Wenker, A., 2003. Resurfacing history of the northern plains of Mars based on geologic mapping of Mars Global Surveyor data. J. Geophys. Res. 108, 8043. http://dx.doi.org/10.1029/2002JE001908.

Turowski, J.M., Rickenmann, D., Dadson, S.J., 2010. The partitioning of the total sediment load of a river into suspended load and bedload: A review of empirical data. Sedimentology 57, 1126–1146. http://dx.doi.org/10.1111/j.1365-3091.2009.01140.x.

Wentworth, C.K., 1922. A scale of grade and class terms for clastic sediments. J. Geol. 30, 377–392.

Williams, R.M.E., Malin, M.C., 2008. Sub-kilometer fans in Mojave Crater, Mars. Icarus 198, 365–383. http://dx.doi.org/10.1016/j.icarus.2008.07.013.

Williams, R.M.E., Irwin, R.P., Zimbelman, J.R., 2009. Evaluation of paleohydrologic models for terrestrial inverted channels: Implications for application to martian sinuous ridges. Geomorphology 107, 300–315. http://dx.doi.org/10.1016/j.geomorph.2008.12.015.

Williams, R.M.E. et al., 2013. Martian fluvial conglomerates at Gale Crater. Science 340, 1068–1072. http://dx.doi.org/10.1126/science.1237317.

Wilson, L., Head, J.W., 1994. Mars: Review and analysis of volcanic eruption theory and relationships to observed landforms. Rev. Geophys. 32, 221–263. http://dx.doi.org/10.1029/94RG01113.

Wilson, L., Chatan, G.J., Head, J.W., Mitchell, K.L., 2004. Mars outflow channels: A reappraisal of the estimation of water flow velocities from water depths, regional slopes, and channel floor properties. J. Geophys. Res. 109, E09003. http://dx.doi.org/10.1029/2004JE002281.

Wolman, M.G., Miller, J.C., 1960. Magnitude and frequency of forces in geomorphic processes. J. Geol. 68, 54–74. http://dx.doi.org/10.1086/626637.

Wood, L.J., 2006. Quantitative geomorphology of the Mars Eberswalde delta. Geol. Soc. Am. Bull. 118, 557–566. http://dx.doi.org/10.1130/B25822.1.

Woodyer, K.D., 1968. Bankfull frequency in rivers. Journal of Hydrology 6, 114–142. http://dx.doi.org/10.1016/0022-1694(68)90155-8.